Record Number: 17210
Author, Monographic: Fortin, J. P.//Bernier, M.//Lapointe, S.//Gauthier, Y.//De Sève, D.//Beaudoin, S.
Author Role:
Title, Monographic: Estimation of surface variables at the sub-pixel level for use as input to climate and hydrological models
Translated Title:
Reprint Status:
Edition:
Author, Subsidiary:
Author Role:
Place of Publication: Québec
Publisher Name: INRS-Eau
Date of Publication: 1998
Original Publication Date: Avril 1998
Volume Identification:
Extent of Work: vi, 118
Packaging Method: pages
Series Editor:
Series Editor Role:
Series Title: INRS-Eau, rapport de recherche
Series Volume ID: 483
Location/URL:
ISBN:
Notes: Rapport annuel 1998-1999
Abstract: Final report to Centre national d'études spatiales (France)
Call Number: R000483
Keywords: rapport / ok/ dl

ESTIMATION OF SURFACE VARIABLES AT THE SUB-PIXEL LEVEL FOR USE AS INPUT TO CLIMATE AND HYDROLOGICAL MODELS

Rapport de recherche N° R-483 *Avril 1998*

ESTIMATION OF SURFACE VARIABLES AT THE SUB-PIXEL LEVEL FOR USE AS INPUT TO CLIMATE AND HYDROLOGICAL MODELS

Final Report

to

Centre national d'Études spatiales

by

Jean-Pierre Fortin
Monique Bernier
Stéphane Lapointe
Yves Gauthier
Danielle De Sève
Stéphanie Beaudoin

Institut national de la recherche scientifique, INRS-Eau
2800, rue Einstein, Case postale 7500, SAINTE-FOY (Québec), G1V 4C7

Rapport de recherche No R-483

Avril 1998

TABLE OF CONTENT

LIST OF TABLES

LIST OF FIGURES

1 OBJECTIVES OF THE INVESTIGATION

The general objectives of the investigation are:

- Estimation of surface variables using data from a medium spatial resolution and high frequency remote sensing sensor in orbit.

- Increased accuracy of spatial registration for multitemporal analysis of data.

Derived from those are the following specific objectives:

- Estimation of physical variables of the surface, corresponding to each land cover within the pixel, the albedo for example.

- Estimation at the sub-pixel level of the spatial distribution of snow cover on the ground.

- As accurate as possible registration of the images for multitemporal input into a spatially distributed hydrological model using geocoded data.

2 APPROACH USED DURING THE PRE-LAUNCH PHASE OF INVESTIGATION

During the pre-launch phase of investigation, the approach has consisted in simulating first VGT and HRVIR data from TM data, the differences in bandwidths being acceptable for our purposes. The other activities were on the development and testing of our methodology on the application of the spectral mixture theory, in order to meet the objectives of the investigation. Development and testing have been undertaken on small simulated VGT images obtained from TM data.

2.1 Simulation of SPOT-4 HRVIR and VGT images

2.1.1 Introduction

Since we estimated that five of the TM bands could be considered as sufficiently good approximations of the bands that we will find for both sensors on SPOT-4 and that it was already a satellite borne sensor, we believed that it was a good basis for simulations of the future sensors. For the moment, we do not believe that small differences in bandwidth and other characteristics of the sensors, like radiometric sensitivity and noise and viewing geometry are crucial for the type of analysis that we intend to perform on the data. The TM2, TM3, TM4 and TM5 bands have been used to simulate the corresponding HRVIR bands, whereas the TM1, TM3, TM4 and TM5 bands were used for VGT. Another advantage of using a satellite borne sensor like TM is simulation of simultaneous data acquisition from the future HRVIR and VGT sensors under the same orbital and atmospheric conditions. On the other hand, simulated VGT images will be relatively small, but it should not be a problem for the type of investigation that we proposed, as actual VGT images will likely have to be subdivided into smaller images in order to respect relatively homogeneous physical variables on the considered area. For instance, any physical variable which is function of latitude will probably have to be estimated for subimages.

2.1.2 Experimental sites

The experimental sites are located in Southern Québec, on the South shore of the St. Lawrence river, and are representatives of the conditions encountered in that region (Fig. 2.1). Various land types can be found, including water surfaces, agricultural fields, waste and wet lands, forested areas

(both conifers and deciduous) and urban areas. One of the image (Nicolet region, 9 May 1993) is taken in spring over a relatively flat area. Another one (Southern Québec, including the St-François to the Chaudière watersheds, 28 August 1995) is a summer image over a more hilly area, while the third one (St.François watershed, 2 April 1988), a little to the South-West of the second one, is an early spring image with partial snow cover over the same type of terrain.

2.1.3 Corrections of atmospheric and directional effects

As anyone knows, reflected radiation from the earth surface in the visible and infrared is affected by various molecules and particules in the atmosphere. Then, for a number of applications, it is advisable, if not necessary,to make a correction for these effects on images from orbiting sensors. Various models have been developed to do that, in particular the LOWTRAN (Kneizys*et al.*,1983), 5S (Tanré *et al.*, 1990)and SMAC (Rahman and Dedieu, 1994) methods. These models need parameters like the vertical visibility, the air temperature and standard air mass characteristics for various types of environments and climates.

In this study, before making any resampling, the TM images have been corrected for atmospheric effects, using the procedure available in the Easy Pace software (Version 6.10 from PCI). This procedure is based on the LOWTRAN-7 (Kneizys *et al.*, 1988) and SENSAT-3 (Richter, 1989) models and assumes that the reflectances from the various surfaces are lambertian and that the terrain is flat. One interesting feature of this procedure is the availability of files containing standard environmental conditions: aerosol types in the atmosphere, solar zenith angle and altitude of the earth surface. This is particularly useful if no actual atmospheric values are available.

As shown in fig. 2.2, the first step consisted in estimating the ground visibility in the atmosphere of the region, using the available files. The US standard atmospheric characteristics for rural environment have been used for that purpose. The next step of the procedure was the transformation of the digital counts into reflectances, without taking into account adjacency effects. A 3 x 3 mean filter was then applied to the data in order to eliminate noise. Finally, an improved reflectance image taking adjacency effects was created.

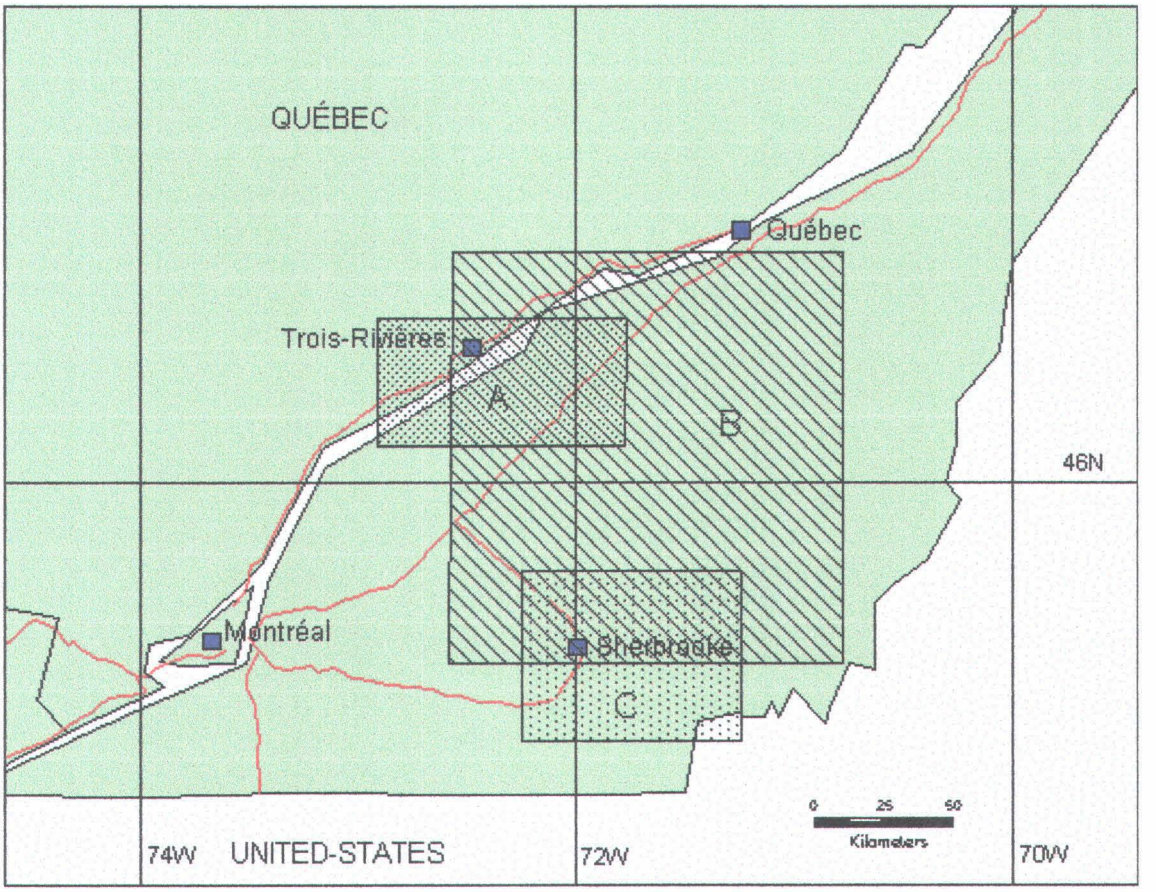

Figure 2.1 Areas covered by each of the three images used in the project

(A) Nicolet - Trois-Rivières region

(B) Southern Quebec, between the St-François and the Chaudière rivers;

(C) St-François watershed

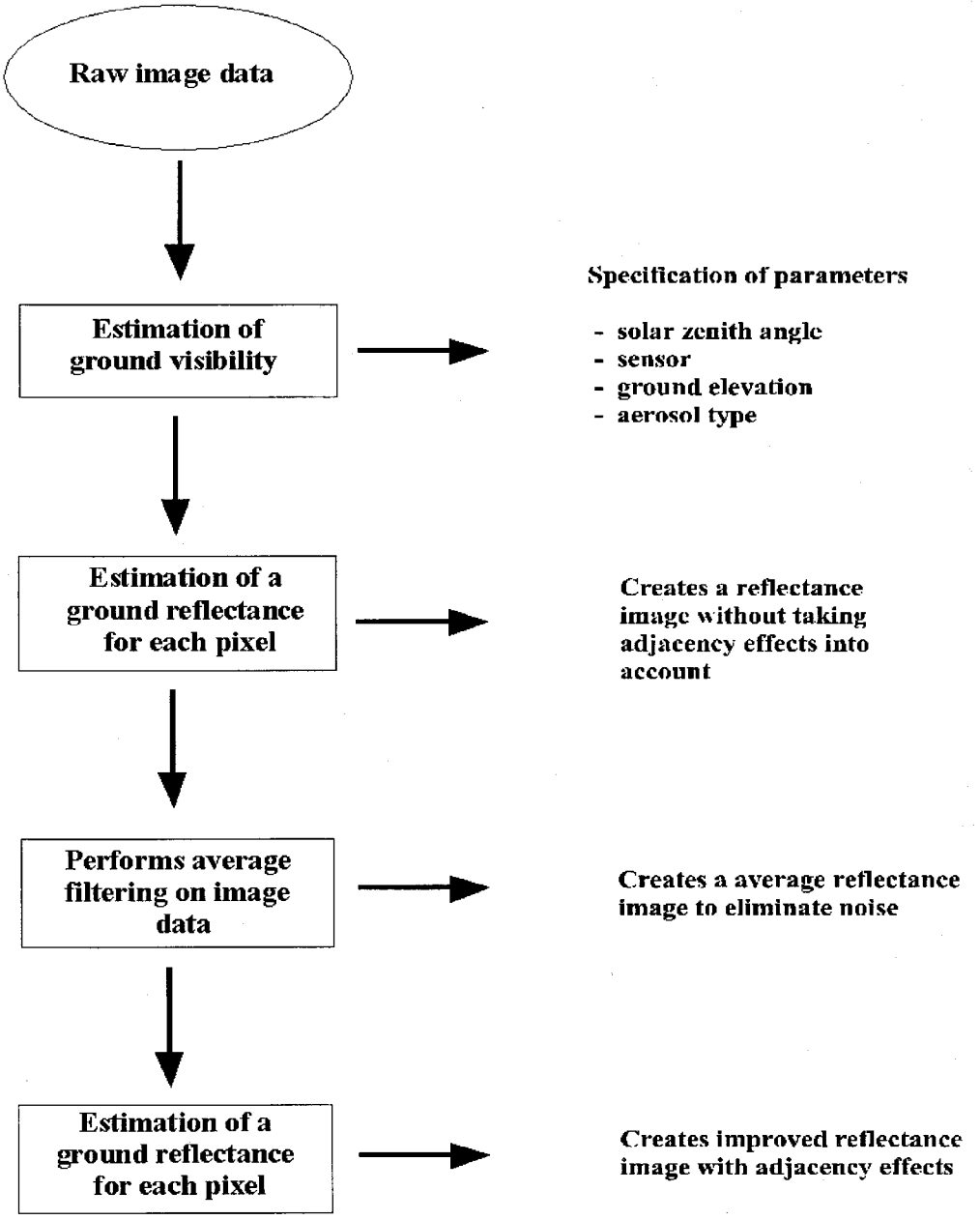

Figure 2.2 Procedure used for correction of atmospheric effects.

The TM images were georeferenced but not corrected for directional effects as the terrain is relatively flat or consists in rolling hills with small slopes and the image is small (narrow field of view). Other directional effects depending on the type of surface are more difficult to correct. For instance, tall vegetation, particularly in the infrared, may have a different reflectance on different images even if the sun and the sensor are in the same geometric position. That variation may come from wind speed and direction. Also, even if one can count on good atmospheric parameters, their spatial representivity is not very large, so that it will be difficult to know if a small reflectance variation is due to directional effects or to differences in atmospheric characteristics.

2.1.4 Simulation of HRVIR and VGT data

After correcting the TM images for atmospheric effects, the next step was the simulation the HRVIR 20-m resolution images. This was made using a nearest neighbor resampling procedure to change the original 25-m geocoded TM data to simulated 20-m HRVIR data. Since both resolutions are approximately the same, it had the advantage of retaining the original digital counts. The simulated 20-m HRVIR data was subsequently used to prepare a land-use classification of the area.

Two methods were retained at the beginning to simulate the 1150-m VGT data. The first one was a simple mean value of 46x46 TM pixel arrays. The second one consisted in modelling "the transfer function between the initial data and the desired data and derive a spatial filter and sampling mechanism to simulate the coarser resolution data from the finer resolution data" according to the procedure suggested by Justice et al.(1989), in which both methods are described. As mentioned by Cherchali (1995), the procedure must, in principle, take the MTF into account, as it represents the modifications made to the actual scene by the various components of the sensor in the image making process. On the other hand, it has been shown that for objects on the earth surface whose dimensions are larger than 60m, the MTF is close to 1 for TM and HRV sensors. One can thus assume, according to Cherchali (1995) and Aman *et al.*(1992) that if he applies "a mean filter to high spatial resolution pixels for a specific surface, he will obtain, for scales larger than 100m a measure corresponding to a MTF practically equal to 1". Also, it can be assumed that environmental side effects become practically negligeable beyond those scales, specially if atmospheric corrections have been done previously. However, if such a filter is used, the noise will be reduced by smoothing of frequency distribution and occurrence of both high and low values will be reduced Aman *et al.*(1992).

Following all those considerations, a 46 x 46 mean filter has been applied to the TM data already corrected for atmospheric effects in order to simulate the VGT data considering that this choice should not affect our results.

2.2 Processing of simulated VGT data for estimation of the mean reflectances of land use classes in a specific geographical area

2.2.1 The spectral mixture approach

According to the spectral mixture theory, the reflectance of a pixel can be considered as the linear weighted mean of the reflectances of the surface elements in the pixel. In our case, the relation between the reflectance of a VGT pixel and that of corresponding HRVIR pixels can be written, for each spectral band, as:

$$R_i = \sum_{j=1}^{n} f_{ij} r_j + \varepsilon_i \qquad 0 \le r_j \le 1 \qquad \textbf{2.1}$$

where : R_i is the reflectance of the VGT pixel i, f_{ij} is the fraction of pixel i occupied by land use class j, r_j is the mean reflectance of land use class j in the considered spectral band, ε_i is an error term for the spectral band taking into account measurement errors and variability of r_j, and n is the number of land use classes.

In practice, we can be interested in finding either the r_j's, that is the mean reflectances in each of the considered spectral bands of the land use classes present on the image, or the f_{ij}'s, that is the fraction of pixel i occupied by each land use class within that pixel. In the first case we may want to estimate albedo, while, in the second, we might be interested in knowing the percentage of snow for each VGT pixel and if possible, for each land use class within that pixel.

2.2.2 General description of the chosen approach.

It can be seen easily that by considering p ($p \geq n$) pixels it is possible to construct an overdetermined equation system which can be solved using a least squares algorithm. The constraints are induced by the fact that the estimated reflectance must be in the interval$[0,1]$. The procedure "non-negative least squares" (nnls) available in MATLAB has been used to solve the system of equations.

It is also necessary to decide which pixels should be selected and, of course, on what criterion. One further question can be asked. Will the selection of only one group of pixels give the best answer or will it be necessary to develop a procedure to select more than one group and if so on what basis?

A general description of the main steps of the proposed approach can be found in Fig. 2.3. The upper part of the figure deals with the simulation of the HRVIR and VGT data (section 2.1.4). Starting with the simulated HRVIR data, it is shown that a supervised classification is made in order to prepare a land use map. Mean reflectances of each land use class for each spectral band are obtained from the original simulated HRVIR image for further comparison purposes. Also, the fractions of each land use class f_{ij} in the VGT pixels are obtained from the map.

Knowing the fraction of each land use class in each VGT pixel, assuming perfect registration, and the reflectances of the VGT pixels, we have to select the pixels and the number of groups of pixels that should furnish the best results using the least squares algorithm. For each group of pixels, VGT reflectances are estimated and, finally, a mean of the reflectances for all groups.

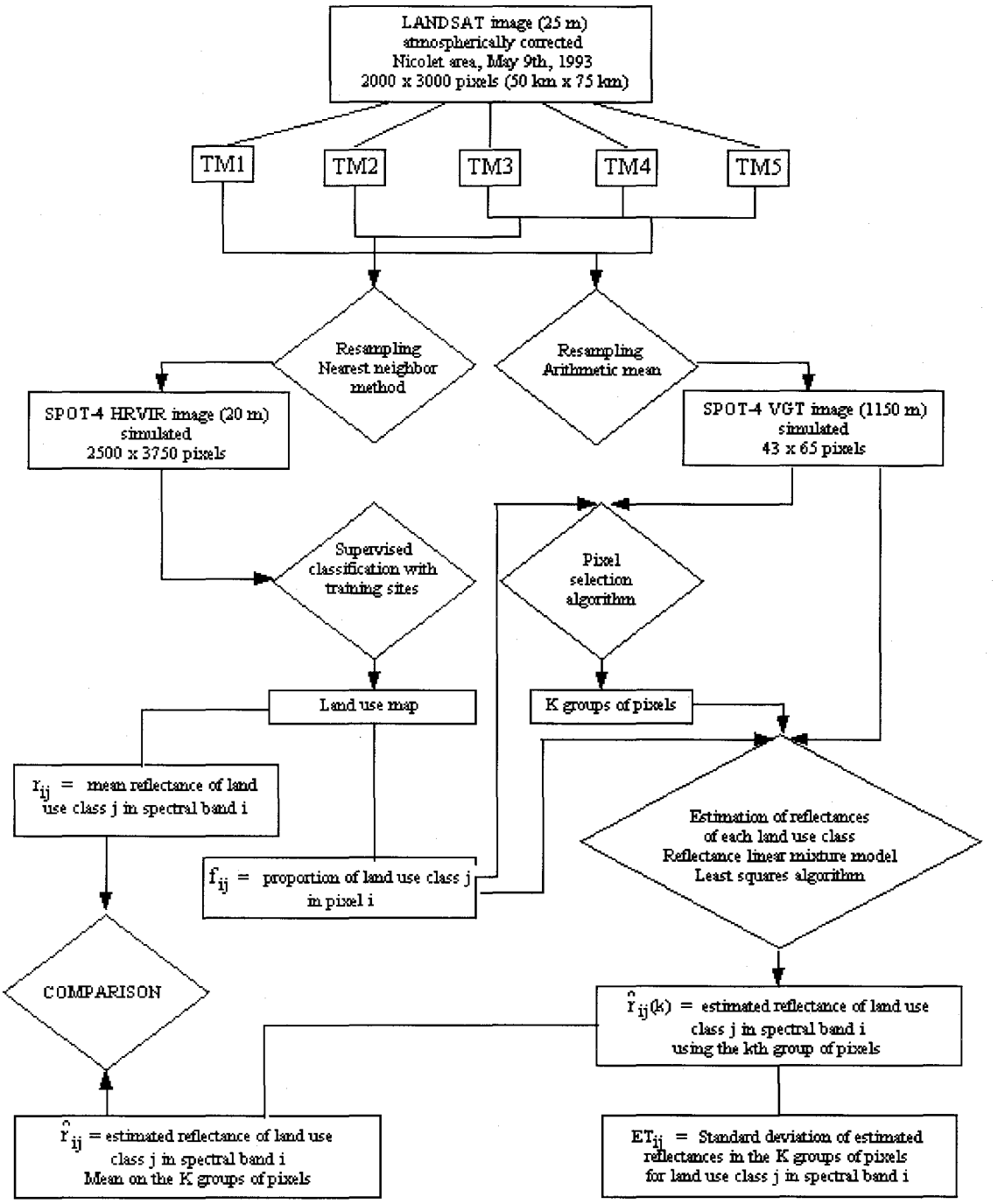

Figure 2.3 Main steps of the proposed approach

2.2.3 Criteria used to evaluate the results

A few criteria are used to evaluate the results. It seems appropriate to describe them immediately.

When mean reflectances of each land use class are known, as it is the case here, the relative error can be used to validate the results. The relative error ER_{ij} in % for band i and class j can be defined:

$$ER_{ij} = \frac{|\hat{r}_{ij} - r_{ij}|}{r_{ij}} 100 \qquad \textbf{2.2}$$

where r_{ij} is the mean reflectance of land use class j for band i, obtained from the HRVIR reflectances and $\hat{r}_{IJ}$ is the estimated reflectance for land use class j and band i from the VGT pixels. If more than one group of pixels are used, the estimated reflectance $\hat{r}_{IJ}$ is the mean of all estimated values.

$$\hat{r}_{ij} = \frac{\sum_{k=1}^{K} \hat{r}_{ij}(k)}{K} \qquad \textbf{2.3}$$

Where K is the number of groups and $\hat{r}_{IJ}$ is the estimated reflectance of land use class j for spectral band i, using group k.

Also, in the case where more than one group are used, the standard deviation Et_{ij} of the estimated values by the various groups for land use class j and spectral band i can be given by:

$$ET_{ij} = \sqrt{\frac{\sum_{k=1}^{K} (\hat{r}_{ij}(k) - \hat{r}_{ij})^2}{K-1}} \qquad \textbf{2.4}$$

Finally, in order to reduce the amount of results, it is interesting to compute mean values according to spectral bands or land use classes. More specifically, we can define the mean relative error by spectral band ($ERMB_i$, where i is the spectral band), the mean relative error by class ($ERMC_j$, where j is the land use class) and the mean standard deviation by band ($ETMB_i$, where i is the spectral band):

$$ERMB_i = \frac{\sum_{j=1}^{N} ER_{ij}}{N} \qquad \textbf{2.5}$$

$$ERMC_j = \frac{\sum_{i=1}^{B} ER_{ij}}{B} \qquad \textbf{2.6}$$

$$ETMB_i = \frac{\sum_{j=1}^{N} ET_{ij}}{N} \qquad \textbf{2.7}$$

where N is the number of classes and B the number of spectral bands.

2.2.4 Selection of pixels

As mentioned in section 2.2.2, our approach consists in selecting K groups of pixels and estimating reflectances for each land use, using these groups and the spectral mixture theory. As slightly different results should be reached using data from these groups, taking the mean of these estimations should lead to even better estimations. In any case, however, the fundamental problem lies in the selection of the pixels for each of these groups. Various criteria can be used to select pixels:

a) Pixels within each group should be selected so that all groups of pixels lead to equally reliable estimations. Otherwise, one should rather consider a weighted mean according to the reliability of the estimations instead of a simple arithmetic mean, when combining estimations coming from the various groups.

b) Each land use class must be well represented in each group to lead to a reliable reflectance estimation, even if possible, for classes representing a small fraction of the image. Ideally, the selected pixels should contain approximately the same percentage of each of these classes.

c) As surface characteristics may vary very much as a function of location in large images, it is advisable to define sub-images in which these characteristics will be sufficiently homogeneous to select pixels whose reflectances will not vary too much. One example of this would be melting snow in the southern portion of a VGT image while the snow is still dry in the northern portion, with temperatures under 0°C.

Let us assume, at the beginning, that only one group of pixels has to be selected and that registration of both information planes (VGT image and land use map from HRVIR data) is perfect. The idea is to select pixels so that we obtain the best possible estimations using only one group of pixels. Of course, we have to select at least as much pixels as there are classes.

Before presenting the chosen selection method, we must define terms that will be used. The best VGT pixel M_j^1 representing land use class j can be defined as the pixel for which f_{ij} is maximum, that is the pixel which "contains" the greatest number of HRVIR pixels of land use class j (if more than one VGT pixel contain the same number of HRVIR pixels for the selected class, a random choice is made between them). The second best pixel M_j^2 in land use class j is the VGT pixel containing the largest number of HRVIR pixels of that class after pixel M_j^1. In the same way, the m-th best pixel M_j^m for class j is the VGT pixel containing the largest number of HRVIR pixels of class j after pixels $M_j^1, M_j^2, \ldots, M_j^{m-1}$.

When only one group of pixels is chosen, the pixel selection procedure consists in choosing first the best pixels in each land use class, $M_1^1, M_2^1, \ldots, M_n^1$, and then n other pixels randomly among the pixels of the VGT image. Thus, 2n pixels are used to solve the system of equations. Completing

the group of n best pixels by n randomly chosen pixels leads to more stable results and to a good reflectance estimation even for less represented classes.

One could discuss the selection of n randomly chosen pixels to complete the group rather than choosing the n second best pixels. Tests were made and the gain in accuracy was not considered significant. Other pixel selection methods have also been tested but lead to less accurate results. For instance, we have considered a method in which all the pixels were randomly chosen while making sure that all classes were relatively well represented by requiring that the chosen pixels had a number of HRVIR pixels higher than a predefined threshold. The selection of pixels in the group was modified until that condition was met. The results were not very satisfying and were very unstable.

To obtain even better results, using the chosen procedure, ten trials are done, keeping the n best pixels but reselecting the random pixels each time. The resulting relative errors are thus mean values of the ten trials.

2.2.5 Optimization of the number of groups

Instead of selecting only one group of pixels, one can consider simultaneously K groups of VGT pixels and proceed to the estimation of the reflectances using each of these groups. Then, the mean of the estimated values in each of these groups will be considered as the estimated reflectance for each class and each spectral band. Taking the mean value helps to reduce the estimation errors made by anyone group. But, how many groups should be chosen to get the best results?

Let us consider the N (number of land use classes) vectors containing the following best pixels (one for each class):

$$\langle M_1^1, M_1^2, \ldots, M_1^K \rangle, \langle M_2^1, M_2^2, \ldots, M_2^K \rangle, \ldots, \langle M_N^1, M_N^2, \ldots, M_N^K \rangle$$

As pixels within each group should be selected so that all groups of pixels lead to equally reliable estimations, the elements of these vectors are randomly swapped, prior to the addition of randomly selected pixels, so that all best pixels are not in the same group. An example will be helpfull. Let us assume that we have four groups and three classes and that the vectors containing the best pixels are:

$$(a_1,a_2,a_3,a_4),(b_1,b_2,b_3,b_4),(c_1,c_2,c_3,c_4)$$

An acceptable permutation would be:

$$(a_3,a_2,a_1,a_4),(b_4,b_1,b_3,b_2),(c_1,c_4,c_2,c_3)$$

This would results in the following four groups of best pixels:

$$(a_3,b_4,c_1),(a_2,b_1,c_4),(a_1,b_3,c_2),(a_4,b_2,c_3)$$

In order to find out the optimal number of groups, the procedure consists in selecting various numbers of groups, from 2 to K, and then, using each one of these k (k=2,K) groups, in proceeding to ten trials with both a new selection of the random pixels and a new permutation of the best pixels. Since the mean reflectances of each class are known it is possible to compare the estimated reflectances to these values and find out how many groups gives the best results.

2.3 Deterioration of estimations with registration errors and possible improvement of geometric accuracy

It is considered in the pre-flight specifications that the multispectral and multitemporal registration errors should be less than 0.1km and 0.3km, if possible. The objective, as far as the absolute location is concerned, is 0.5km. With this in mind, we have looked at the degradation of the results as the registration error goes from 0 to 300m. Also, as k groups of pixels should furnish more and more relatively identical reflectance estimations as the registration becomes more and more

accurate, we tried to find a way to have more accurate registration as a side product of the reflectance procedure, using an optimal number of pixel groups.

2.3.1 Deterioration of estimations with registration errors

In order to analyse the deterioration of estimations with registration errors, we assumed that there was a shift between the actual location of the VGT image and that of the land use map obtained from HRVIR data. More precisely, we considered shifts of -300m,-200m, -100m, 0m, 100m, 200m, 300m in the East-West direction as well as in the North-South direction. New VGT images corresponding to these shifts were generated. The estimated reflectances for each land use class and each spectral band, as obtained from the shifted VGT images, were compared to the estimated reflectances assuming perfect registration, in order to analyse how the relative error grew with increasing distance from the assumed true position. That type of analysis has been done only on the first simulated images, that of the Nicolet region.

2.3.2 Possible improvement of geometric accuracy in an operational procedure

In an operational context, the registration errors will be unknown but should be within the expected values. Also, normally it will not be possible to compare the reflectances estimated from mixed VGT pixels to those of pure HRVIR pixels taken at the same time. One exception will be the area covered by both VGT and HRVIR images when both images are taken at the same time, but even in that case there is the possibility of a colocation error of 300m.

There is still a possibility to find out a best match between the land use map and a VGT image for which the registration error is unknown. As it is not possible to modify the reflectances of the VGT image, in that case, we will shift the grid superimposed on the classified HRVIR image for estimation of the percentages of each land use class in the VGT pixels. By doing so it will be possible to create percentages of land use classes for various shifts, one of these shifts being that of the VGT image. The reflectances for each land use class and each spectral band are then computed in the same way as in 2.2.2, using k groups of VGT pixels. In practice, the true shift will be unknown. However, it should be remembered that our method consists in taking the mean of the estimations made by each of the k groups. Then, it is possible to compute the standard

deviation of these estimations. The most probable shift should be the one for which the standard deviation is the smallest. Using that criterion, it should be possible to obtain a better registration accuracy.

In practice, two methods were used to perform the search for the best accuracy. The first one consists in an exhaustive procedure similar to the one used in 2.3.1. As mentioned above, the grid superimposed on the classified HRVIR image is shifted in both directions, this time with a distance increment of 50 m, to find out the location where the lowest standard deviation for reflectance estimation is reached. It should be understood that as the fit between the position of the classified HRVIR image and the VGT image becomes more and more accurate the values of the reflectances estimated from any of the K groups of pixels should become more and more identical, such that the standard deviation between estimations becomes smaller and smaller.

The second one is an heuristic hill-climbing procedure. As in the previous procedure, both a search distance and distance increment have to be defined. As, the 300m colocation error does not lead in practice to a square but to a circle, the estimated 300m colocation error has been taken as the radius of that circle and a distance increment of 20m has been chosen. In that procedure, the standard deviation is first estimated at five locations: at the center of the circle (perfect registration assumed) and at the center of the four quadrants obtained by dividing the circle in the North-South and East-West directions by lines crossing each other at the center of the circle. The location corresponding to the lowest standard deviation is selected at the end of this first round. Next, using that location as the center of a new search, estimations of the standard deviations are made at locations 20m from that new center along the four directions. Again, the location corresponding to the lowest standard deviation is selected and the process is repeated as long as it is still possible to reduce the standard deviation. Normally, this procedure is less time consuming than the first one, but one should be aware of the possibility of reaching a local minimum, thus missing the desired minimum and registration accuracy. However, it is possible to verify if the minimum reached is local or not and solutions to find out the needed minimum are available. In the case of VGT images, four spectral bands will be available. The estimated misregistration between bands for a specific image being not more than 100m , the locations estimated for each of the four spectral bands should be relatively close to each other. If this is not so, the possibility of at least one

location being that of a local minimum is there. The first solution consists in rerunning the program to find out a new solution, based on the random selection of pixels. This could be a good way to verify the first results and make any necessary correction. A second solution consists in selecting new starting locations to initiate the procedure.

2.4 Processing of simulated VGT data for the estimation of the percentages of snowcover present in each broad land use class of any VGT pixel in a specific geographical area

2.4.1 The spectral mixture approach in the case of a VGT image with partial snow cover

In the general case where the needed variable is the percentage p_{ij} of occupation of each land use class in each pixel rather than the mean reflectance of those classes, as it was the case in section 2.2, equation 1 is still applicable (Simpson *et al.*, 1998). However, in that case the number N of possible land use classes, or endmembers, is limited by the number of uncorrelated spectral bands available, that is more uncorrelerated bands than endmembers are required (Kerdiles and Grondona, 1995; Shimabukuro *et al.*, 1997; Novo and Shimabukuro, 1997). Kerdiles and Grondona (1995) explain that it is possible to incorporate various dates to obtain more bands than endmembers. However, they mention that the percentages p_{ij} must be constant over the selected dates and that the endmember reflectances must be known.

Let us now consider a VGT image with a partial snow cover. Because of the dimensions of a VGT pixel, more than one or two land use classes can be present on it at the same time. Is it possible to estimate the percentages of snow cover over each of the land use classes present on a specific pixel? Theoretically, the answer is yes, provided that the above conditions are respected. On the

other hand, if problems arise to find out a solution to the above question, is it possible to find out at least the total percentage of snow cover on that pixel?

A possible solution to the first question could come from one of our objectives which is to use the resulting snowcover map as input to hydrological models, and more specifically to our distributed model,HYDROTEL. For snow accumulation and melt, the actual land use classes present on a watershed are integrated into only three broad classes: coniferous forests, deciduous forest and open areas. A fourth class could be added to the first three, that of water bodies. On the other hand, only four spectral bands are available on a VGT image and the VGT1 and VGT2 bands are relatively highly correlated. As the number of sufficiently uncorrelated spectral bands limits the number of land use classes to three, an approach making use of more than one spring image should normally be developed.

We first need to know the percentages of the above classes under snow free conditions and the corresponding spectral signatures under the same conditions. We further need to know the spectral signatures of those classes under the snow cover conditions possible during the melt period. If HRVIR images are used, the percentages of these classes under snow free conditions can be known from either images taken in fall after the leaves are fallen in deciduous forests and before there is any snow on the ground in the region of interest or spring images taken after complete snowmelt. It could also be possible to use HRVIR images with partial snow cover. Then, those percentages will be obtained by adding together the percentages of the same class with and without snow for the specific date on which the image was taken. The percentages could also come from combined VGT and HRVIR images according to the procedure that will be outlined for operational purposes, in chapter 7 of this report.

As far as spectral signatures are concerned, HRVIR or VGT images taken in fall or in spring to determine the percentages occupied by each of the needed land use classes could also be used to estimate spectral signatures for snow free conditions. HRVIR images allowing estimation of spectral signatures of snow covered areas at the beginning and during the melt period but also of fresh new snow during that period, should also be taken, if possible, at appropriate dates. It should be mentioned that the spectral signatures of various types of snow covered open areas would likely

be relatively similar, due to the reflectance of snow. That will not be the case for the same open areas under snow free conditions, as bare fields and pastures, for instance, will not have the same signatures.

Then, in the case where the percentages of snow covered areas are needed for each of the four selected land use classes and the reflectances are known, the spectral mixture equation can be written:

$$R_i = R_{i_f} + \sum_{J=1}^{N} p_{ij_s} (r_{j_s} - r_{j_f}) + \varepsilon_i \qquad \textbf{2.8}$$

where:

$$R_{i_f} = \sum_{J=1}^{N} p_{ij_f} r_{j_f} \qquad \textbf{2.9}$$

and:

R_i = reflectance of VGT pixel i with a possible snow cover from 0 to 100%;

R_{if} = reflectance of VGT pixel i under snow free fall conditions;

r_{js} = reflectance of land use class j under snow cover conditions;

r_{jf} = reflectance of land use class j under snow free fall conditions;

p_{ijs} = percentage of pixel i occupied by land use class j, with snow cover conditions;

p_{ijf} = percentage of pixel i occupied by land use class j, under snow free conditions;

ε_i = error term for the spectral band taking into account measurement errors and variability of r;

N = number of land use classes.

In practice, problems will likely be encountered as both reflectances of land use classes and the percentages of snow covered area over each of the total area occupied by each land use class change rapidly during the snowmelt period. It is unlikely that HRVIR images could be obtained every few days, particularly if cloud cover is taken into account. So, they cannot be used alone to monitor snowmelt. In the case of VGT images, it should be possible to monitor the variation of reflectance of the land use classes while the snow cover is still complete, as the percentage of each land use will remain constant for that period. VGT images could also permit monitoring of the reflectance of the land use classes during the melt period, as long as only a few classes are present at the same time on a specific pixel and the percentages of snow cover on each land use class is known. As far as finding the percentages of snow cover for each land use class, it is likely that at least a few images will be necessary. A "cold" period with no or very little snowmelt, during which the percentage of snow cover does not change very much over each of the land use classes, could allow such estimation. The variation of reflectance during that short period could then come from a model.

Another solution can, however, be put forward as a single spring image could be used to find out the total percentage of snow cover on each pixel with a relatively good accuracy. Once that percentage is done, it could be possible to distribute that percentage among the various land use classes, knowing that snow will disappear first in open areas, then in deciduous forested areas and finally in coniferous forests. As the resulting partial snow cover map will, at least in a few applications, be used to update the snow cover in a hydrological model for snowmelt forecasting, the informations furnished by that model could, in turn, help to distribute the total snow covered area on each pixel among the land use classes present on that pixel.

Two indices are suggested to find out the total snow covered areas on each pixel. Both are based on the effect of the snow reflectance on the ground cover as compared to snow free reflectances of the various land uses. Let us first remember that equation 2.9 gives the relation between the endmember reflectances and the VGT pixel reflectance for snow free conditions, either in fall of in spring. A similar equation can be written for complete snow cover conditions for the same land use classes.

$$R_{i_s} = \sum_{J=1}^{N} p_{ij_s} r_{j_s} \qquad \textbf{2.10}$$

Where:

R_{is} = reflectance of VGT pixel i under snow cover conditions;

r_{js} = reflectance of land use class j under snow cover conditions;

p_{ijs} = percentage of pixel i occupied by landuse class j, with snow cover conditions;

N = number of land use classes.

Finally, the reflectance of pixel i under partial snow cover conditions is given by equation 2.8. It is then possible to suggest a first relation:

$$F = \frac{R_i - R_{i_f}}{R_{i_s} - R_{i_f}} \qquad \textbf{2.11}$$

It can be seen rapidly that, for a given pixel, F will go from a value of 1, when the snow cover is complete and the reflectances of the land use classes are identical to those used at the denominator, to a value of 0, under snow free conditions identical to those used for the fall or spring reference image. The value of F between those two extremes will be a function of the amount of snow cover on each of the land use classes present on the pixel, as it can be understood from equation 2.8.

A relation similar to the NDVI, which we will call the normalized difference snow index, NDSI, can also be derived:

$$NDSI = \frac{R_i - R_{i_f}}{R_i + R_{i_f}} \qquad \textbf{2.12}$$

The effective relation between those two indices and the total snow cover on each pixel will be shown in chapter 6.

2.4.2 Description of the chosen approach

In the case of partial snow cover when the needed variable is the fraction of snow cover on each individual pixel or, if possible, the fraction of snow cover for each of the land use classes present on the pixel, the chosen approach is similar to that shown in figure 2.3. In practice, we still have to find out first the true position of the VGT image as accurately as possible. For this purpose, we use the same procedure as described before, but with a modification. Remembering that we have a VGT image with a partial snow cover, we use 2 x K groups of pixels, K groups on the completely snow covered portion of the image and K groups on the completely snow free portion of the image. These portions will normally be determined by visual inspection of the image, knowing the effects of snow cover on reflectances. In practice, one can also use histograms for each land use classes and/or informations coming from a simultaneous HRVIR image. Completely snow covered or snow free pixels should be chosen in order to be able to apply the procedure shown in figure 2.3, which rely on the estimation of reflectances of land use classes, knowing the percentages of these classes on each of the chosen pixels.

Once the position of the VGT image will be known as accurately as possible, it will be possible to proceed to the estimation of percentages of snow cover on a pixel by pixel basis.

3 SIMULATIONS TECHNIQUES AND THEIR IMPACT ON DATA QUALITY, RELATIVELY TO EXPECTED VGT DATA QUALITY

As mentioned previously, TM data have been used to simulate both HRVIR and VGT data, as it was considered a good compromise to simulate simultaneous data acquisition from those sensors, when in orbit. The respective spectral bands are presented in Figure 3.1 and Table 3.1 (together with a few more informations on the sensors).The pre-flight specifications are that "the spectral bands of the two instruments should be as similar as possible, the relative difference between measurements on the same object being not more than 3%". The spectral bands are thus assumed identical in Fig. 3.1, in agreement with the more recent informations on the WWW VGT site.

Table 3.1 TM, HRVIR and VGT characteristics

	Landsat-TM	**HRVIR**	**VGT**
spectral bands (um)	0.45- 0.52 0.52- 0.60 0.63- 0.69 0.76- 0.90 1.55- 1.75 10.4-12.50 2.10- 2.35	-- 0.50-0.59 0.61-0.68 0.79-0.89 1.58-1.75 0.61-0.69 (p)	0.43-0.47 -- 0.61-0.68 0.79-0.89 1.58-1.75
Spatial resolution	30 m TM1-TM5 et TM7 120m TM6	20 m XS 2,3,4 10 m XS 1	1150 m
Local hours	9 h 30	10 h 30	10 h 30
Swath width	185 km	60 Km 117Km	2250 km
Temporal resolution	18 days	26 days	1 or 2 / day(s)

The following comments will be made in relation to the objectives of our project. As seen in Figure 3.1, the TM1 band is shifted toward longer wavelengths in comparison with the VGT1 band, as is the TM2 band compared to the HRVIR1 band. The other three TM bands are more similar to the corresponding HRVIR and VGT bands. The TM5 band, however, is larger than the HRVIR4 and VGT4 bands. A comparison, made by Guyot and Gu (1994),of SPOT-HRV and LANDSAT-TM data taken on the same day,indicates that the TM2 band leads to reflectances higher than those estimated for XS1 (HRVIR1) data for all targets in the image, the largest difference being obtained for bare soils at around 3%, most differences being lower than 1%. In the red, the shift of the TM3 band leads to reflectances of water surfaces being lower than those of the corresponding XS2 (HRVIR2) band, whereas the reflectances are practically the same for bare soils and other surfaces. Finally, the TM4 and XS3 (HRVIR3) bands give relatively similar results. They add that the dynamic range of the TM sensor in the green is lower than that of SPOT, which means that it might be more difficult to discriminate some surface features with the TM sensor than with the SPOT sensor in that band. The dynamic range is better in the red but still a little lower than that of SPOT. In the infrared, the TM sensor is a little better than the SPOT sensor.

Spectral reflectances of vegetation, soil and snow that we have seen in the TM5, VGT4 range seem to lead to a conclusion that the use of the TM5 band to simulate the VGT4 and HRVIR4 data should not affect very much the discrimination of such surface characteristics, as well as reflectance estimations.

Also, since we are simulating both VGT and HRVIR data from TM images, we did not encountered significant directional effects. However, we expect to find out such effects on real VGT images.

In short, we do not believe that the discrepancies between the TM spectral bands and those of the HRVIR and VGT sensors will be a problem for the methodology that we are developing. Also, normally, the real data should give even better results.

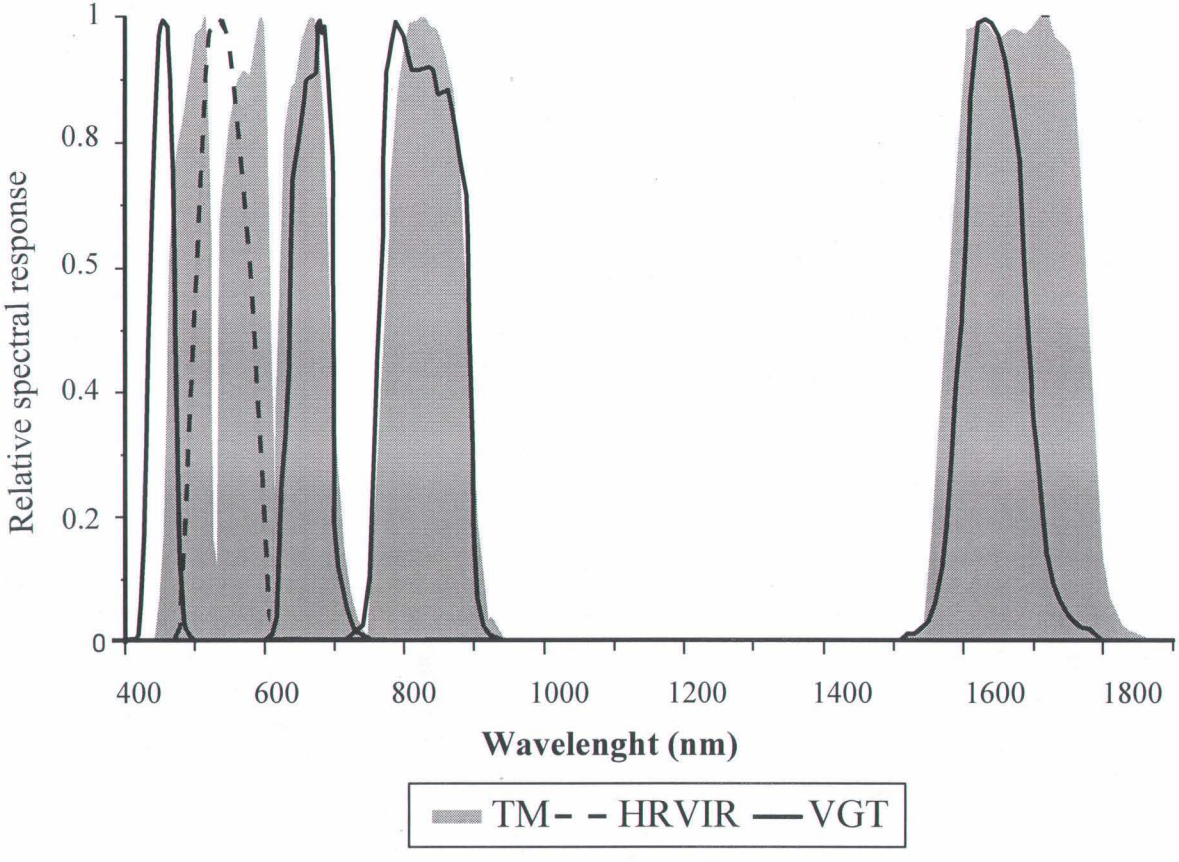

Figure 3.1 Relative spectral responses of TM, HRVIR and VGT bands

4 ESTIMATION OF LAND USE REFLECTANCES FOR THE NICOLET - TROIS-RIVIÈRES REGION

4.1 Visual and statistical evaluation of the simulated HRVIR and VGT images

The experimental site is located in the Nicolet - Trois-Rivières region, half-way between Quebec City and Montreal, on both sides of the St. Lawrence river (Fig. 4.1) and includes the types and spatial distribution of land use classes found in Southern Quebec. The TM image has been taken on the 9th of May 1993 at 9:30 a.m.(local time) and covers a 75km x 50km relatively flat agricultural region. Soil types are mainly sand and clay. Peat bogs can also be found, together with wet lands. On the north shore, the region is crossed by rivers, in particular the Petite rivière du Loup, the Yamachiche and the St. Maurice river, the largest. On the south shore, the main rivers are the St. François, the Nicolet and the Bécancour rivers.

The simulated HRVIR image is shown in Fig. 4.2, while the simulated VGT image is presented in Fig. 4.3. Color composites of bands 2, 3 and 4 are presented for both HRVIR and VGT data on Fig. 4.3. If we have a look at the St. Lawrence river tributaries on the north shore as well as on the south shore, we can easily see that for the HRVIR image, the "Petite rivière du Loup, the Yamachiche and the St.Maurice rivers can be identified on the north shore, while the St.François, the Nicolet and the Bécancour rivers can be identified on the south shore. Of course, it is much easier to identify the rivers on the HRVIR4 band than on the shorter wavelength bands, as the contrast between water and other surfaces is higher in this band. The rivers can also be seen on the HRVIR color composite.

The VGT image has much larger pixels but still, on bands VGT3 and VGT4, it is possible to identify the St.Maurice River on the north shore and the St.François on the south shore. The same is true on the color composite.

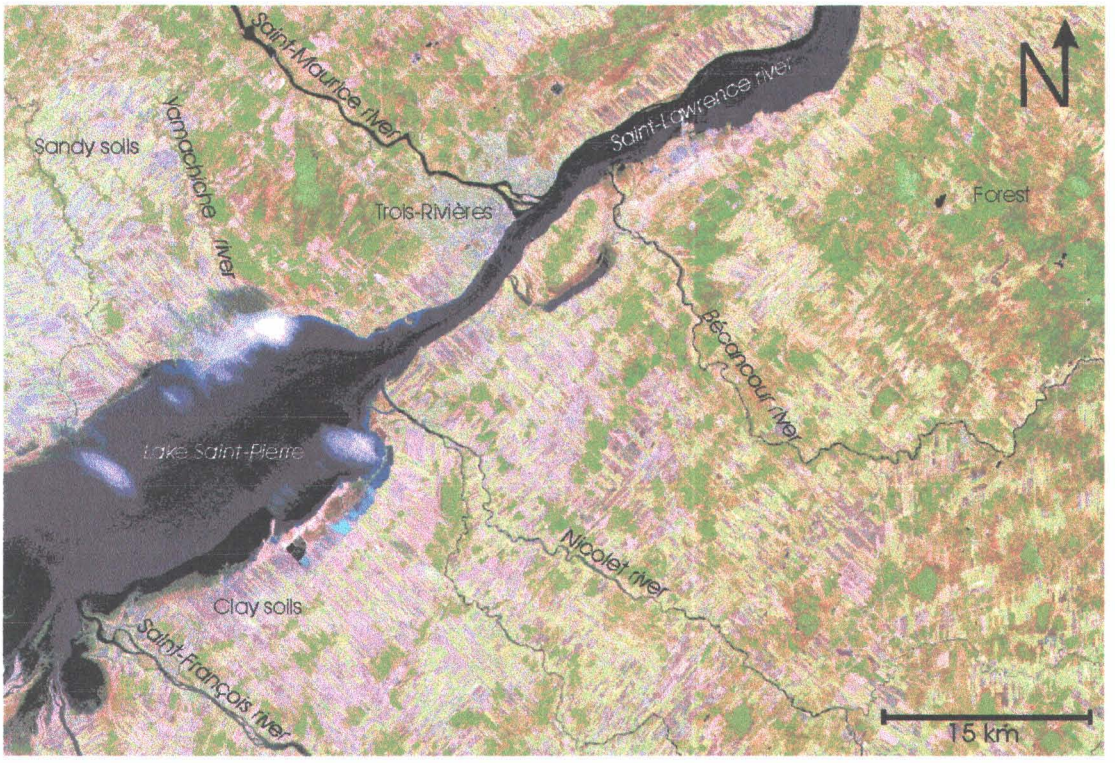

Figure 4.1 Original TM image (TM5, TM4, TM3 - May 9, 1993) for the Nicolet - Trois-Rivières region

Looking now at the St.Lawrence river, we can see that its width seems to increase from VGT1 to VGT4, as a function of the contrast between water and other surfaces. As a matter of facts, its width on VGT4 corresponds more to that which can be estimated on the HRVIR data, no matter what band. Also, in the VGT1 and VGT2 bands, it is possible to distinguish various types of water, particularly in Lake St.Pierre. More specifically, along the shore of the lake, the waters of the St.François river, as well as those of two more rivers flowing into the lake in the extreme south-west corner of the image, can be cleary distinguished.

Urban and industrial areas can also be identified, mostly due to their higher reflectance properties. It is also possible to identify sandy and clay soils. The sandy soils have reflectances higher than the clay soils and are probably drier.

As it can be seen on the HRVIR image, a few clouds can be noticed over Lake St.Pierre.

Finally, as shown in Table 4.1, the mean reflectance and standard deviation values for the original TM image, corrected for atmospheric effects, and for the simulated VGT image, behave as assumed in each spectral band. The mean values are practically identical, while the standard deviations for the simulated data are smaller than those of the original data. As mentioned previously, this is a consequence of the simulation process. We should find out less extreme values in the simulated data than in the original. However, even with a much better simulation process, the extreme values would still be smaller than those from the high resolution sensor, because they would be the result of some sort of averaging process.

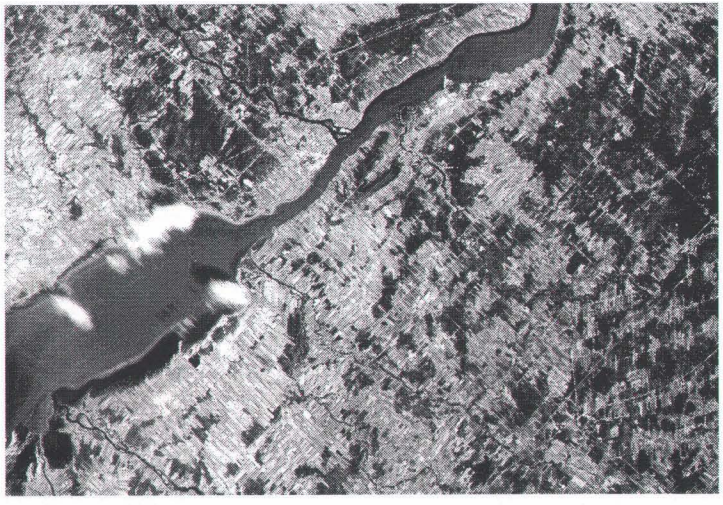

HRVIR1

HRVIR2

HRVIR3

HRVIR4

Figure 4.2 Simulated VGT bands - May 9, 1993

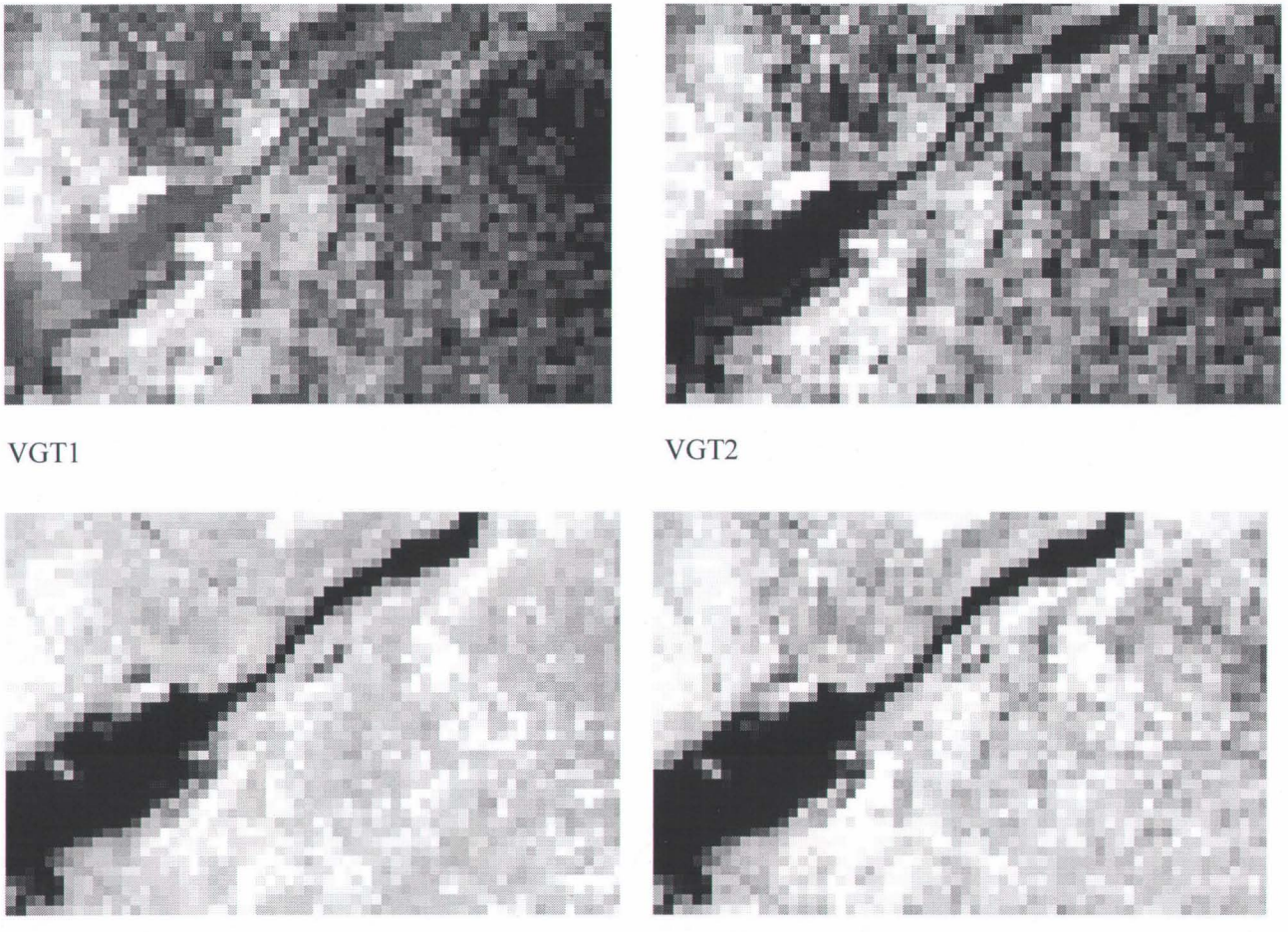

Figure 4.3 Simulated VGT bands - May 9, 1993

a) HRVIR bands (HRVIR1, HRVIR2, HRVIR3)

b) VGT bands (VGT3, VGT2, VGT1)

Figure 4.4: Simulated false color composites of HRVIR and VGT bands - May 9, 1993

Table 4.1 Comparison of mean reflectance values of TM and VGT bands, with standard deviation

	Landsat TM	VGT
	TM1	**VGT1**
Mean	14.44	14.12
Standard deviation	07.43	06.23
	TM3	**VGT2**
Mean	29.30	29.31
Standard deviation	13.02	09.66
	TM4	**VGT3**
Mean	69.29	69.07
Standard deviation	27.48	23.10
	TM5	**VGT4**
Mean	70.61	70.51
Standard deviation	32.27	26.72

4.2 Classification results

In order to define the percentages of each land use class present in each VGT pixel, the HRVIR image has been classified according to the Maximum Likelyhood algorithm, using training sites and the simulated HRVIR bands (figure 4.5). As it was covered by clouds or cloud shadows, 1.5% of the image was masked for the classification. A few statistical results on the classification are presented in Table 4.2. Ten land use classes have been selected, of which two are not well represented: wet lands (0.9% of the image) and peat bogs with alders (0.4%). All other classes occupy at least 2.5% of the image, the highest percentage being for pastures, alfalfa and hay with 21.5%. The statistics for the "cloud" class should be taken into account as that class is made out of cloud, cloud shadows and a few surface features attenuated by thin clouds. Both the mean reflectance and standard deviation values seem to be generally correct.

The coefficient of variation (standard deviation/mean) is greater than 0.5 for "water". This can be explained. As mentioned above, various types of water are present in Lake St.Pierre, but no distinction was made among them.

Table 4.2 Mean reflectance and standard deviation values of simulated HRVIR data for each land use class

Land use	% of total	Reflectance HRVIR1		Reflectance HRVIR2		Reflectance HRVIR3		Reflectance HRVIR4	
classes	land use	mean	std dev.	mean	std dev.	mean	std dev.	mean	std dev.
Water	**13.2**	**2.8**	1.4	**4.1**	2.1	**3.8**	2.3	**2.4**	1.4
Dry bare soils	**12.0**	**6.3**	1.4	**13.0**	2.0	**21.4**	2.3	**26.9**	3.1
Wet bare soils	**6.7**	**4.9**	1.1	**9.8**	1.5	**15.7**	1.8	**18.7**	2.3
Pastures, alfalfa and hay	**21.5**	**4.1**	0.9	**8.7**	1.5	**25.7**	2.9	**25.4**	2.5
Forested areas	**16.6**	**2.0**	0.7	**4.6**	1.1	**18.5**	1.9	**14.1**	2.9
Wet lands	***0.9***	**3.3**	0.9	**5.9**	1.2	**12.3**	2.4	**10.4**	1.8
Peat bogs with spruces	**2.5**	**1.8**	0.4	**4.7**	0.4	**19.4**	1.7	**14.7**	0.9
Peat bogs with alders	***0.4***	**2.2**	0.5	**5.0**	0.6	**11.4**	1.5	**15.3**	3.2
Herbaceous fallow lands and bushes	**15.6**	**2.6**	0.7	**6.3**	1.2	**17.9**	1.9	**21.2**	2.6
Urban areas and roads	**10.6**	**4.6**	1.7	**9.1**	2.3	**18.1**	3.2	**19.6**	3.1
Clouds	**1.5**	**8.6**	4.0	**12.4**	4.6	**16.7**	5.8	**16.5**	7.0

4.3 Estimation of class reflectances from one group of pixels

Using the pixel selection procedure described previously in 2.2.4, ten trials were made with a new selection of random pixels each time, assuming perfect registration between the high resolution land use classification and the VGT image. Thus, the relative errors presented in Table 4.3 are the mean values of these ten trials.

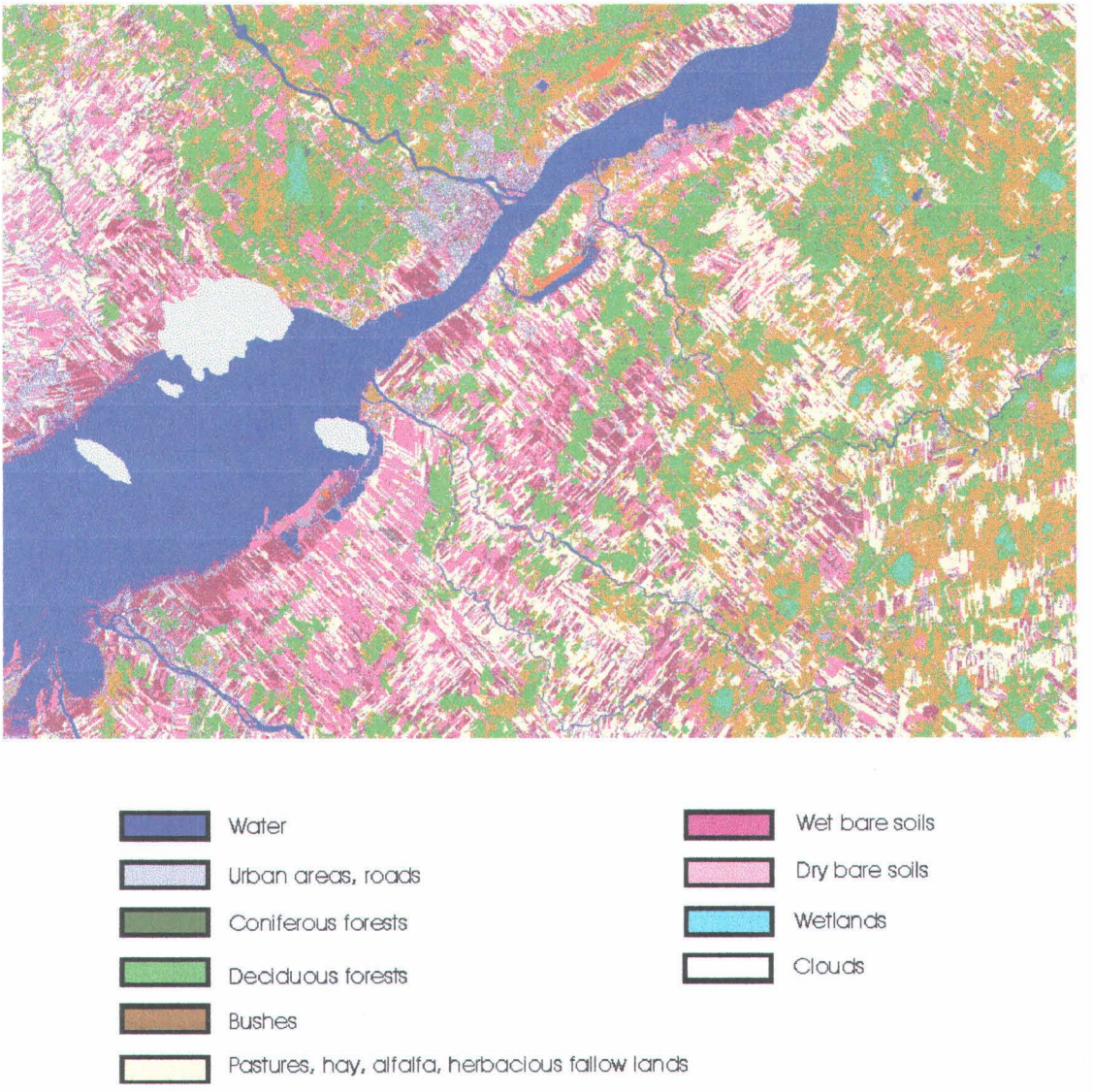

Figure 4.5 Classified HRVIR image - May 9, 1993

Table 4.3 Relative error for reflectance estimation using one group only, mean value for ten trials using 10 best pixels, plus 10 random pixels

Land use classes	**VGT1**	**VGT2**	**VGT3**	**VGT4**	**Mean by class**
Water	26.9	13.2	6.4	7.7	**13.5**
Dry bare soils	16.9	12.2	1.1	6.7	**9.2**
Wet bare soils	10.8	3.2	2.2	5.7	**5.5**
Pastures, alfalfa and hay	7.2	3.2	7.0	1.2	**4.7**
Forested areas	41.3	26.2	1.6	19.4	**22.1**
Wet lands	49.6	32.1	39.3	42.7	**40.9**
Peat bogs with spruces	16.0	1.1	2.7	1.6	**5.3**
Peat bogs with alders	45.3	27.8	28.6	8.7	**27.6**
Herbaceous fallow lands and bushes	20.1	9.7	7.5	2.4	**9.9**
Urban areas and roads	39.5	19.4	7.1	4.4	**17.6**
Mean by spectral bands	**27.4**	**14.8**	**10.4**	**10.0**	**15.6**

Let us look first at the relative errors for each band. We can readily notice that the errors are larger for the VGT1 band and decrease with increasing wavelength. This can be explained by the definition of the relative error and the values of the reflectances in the various bands. Reflectances in the simulated VGT1 band are the lowest and increase from that band to the VGT3 and VGT4 bands. A same absolute error will thus correspond to a larger relative error for the VGT1 band than for the VGT3 or VGT4 bands. In practice, the estimated values are normally within one standard deviation from the mean HRVIR reflectances for each class.

As expected, the relative errors by class vary as a function of the area occupied by that class on the image. The errors are larger for classes occupying only a small percentage of the image, for instance the classes wet lands and peat bogs with alders. For these classes, the estimations are outside the standard deviations of the high resolution data. Otherwise, they are normally within one standard deviation, which is acceptable.

4.4 Optimal number of groups for the estimation of class reflectances

When more than one group of pixels are chosen, more than one best pixels have to be identified for each class, as explained in 2.2.5. A maximum of ten groups was considered. Table 4.4 presents the percentages of land use classes present in each of those pixels. As seen in the table, with the exception of the two less represented classes on the image, the "wet land" and "peat bogs with alders", the percentages of occupation are all relatively high, even for the 10th best pixel.

Table 4.4 Percentages of the land use classes in the ten best VGT pixels for each class

	Land use									
classes	**Max 1**	**Max 2**	**Max 3**	**Max 4**	**Max 5**	**Max 6**	**Max 7**	**Max 8**	**Max 9**	**Max 10**
Water	100%	100%	100%	100%	100%	100%	100%	100%	100%	100%
Dry bare soils	83%	80%	79%	79%	76%	76%	74%	72%	72%	71%
Wet bare soils	94%	80%	76%	74%	73%	70%	69%	66%	62%	61%
Pastures, alfalfa and hay	89%	89%	87%	86%	84%	84%	83%	82%	81%	80%
Forested areas	92%	91%	89%	89%	89%	89%	88%	88%	87%	84%
Wet lands	36%	34%	32%	30%	30%	29%	29%	28%	26%	26%
Peat bogs with spruces	95%	85%	82%	79%	66%	55%	52%	48%	48%	47%
Peat bogs with alders	44%	40%	36%	33%	28%	17%	14%	12%	12%	12%
Herbaceous fallow lands and bushes	92%	92%	89%	88%	86%	83%	83%	83%	81%	81%
Urban areas and roads	78%	75%	74%	73%	73%	71%	68%	68%	67%	66%

In order to find out the optimal number of groups of pixels, ten trials have also been made, each time with a new selection of random pixels and a new permutation of the best pixels in the vectors defined by the number of groups. The mean relative errors resulting from the ten trials, for each of the bands, are presented in fig. 4.6.

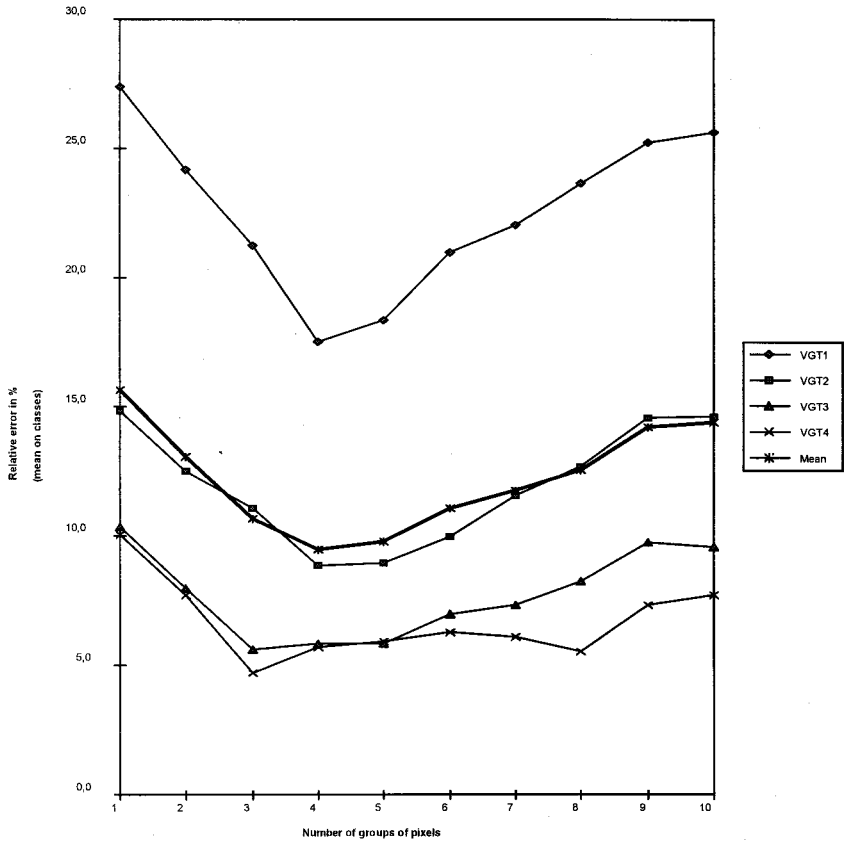

Figure 4.6 Relative error (%) for each VGT band, as a function of the number of pixel groups. Mean on the land use classes and ten trials.

It can be seen that the relative errors diminish rapidly at the beginning as the number of groups is increased, reach a minimum and increase again if the number of groups is further increased. The optimal number of groups is found to be 4 for the VGT1 and VGT2 bands and 3 for the VGT3 and VGT4 bands. As the improvement is greater for the first two bands, the mean relative error considering the four bands, leads to 4 as the optimal number of groups, if all bands are processed at the same time. Whereas the mean relative errors by band were 27.4%, 14.8%, 10.4% and 10.0% for bands VGT1 to VGT4, using only one group, they fell to 17.5%, 8.9%, 5.8% and 5.7% using four groups, a mean decrease of 39%.

One could ask why the mean relative error does not continue to diminish as the number of groups is increased? In order to answer, it is necessary to come back on the best pixel selection procedure. As the number of groups is increased, the supplementary best pixels that have to be identified are bound to contain lower percentages of the specified land use class than the previously identified pixels, as shown in Table 4.4. As pixels within each group should be selected so that all groups of pixels lead to equally reliable estimations, the elements of these vectors are randomly swapped,as explained in 2.2.5. So, permutation of the best pixels will have as a consequence, as the number of groups increases, that pixels containing a lower percentage of a specified class will be included. This will lead to an overall lower quality of the groups as their number increases.

For a small number of groups, as the identified best pixels should still represent relatively high percentages of the specified land use class (they do in the present case), taking the mean of the values will more than compensate the use of nth best pixels (n is 2, 3 and 4 in our case). However, as the number of groups increases that will not be the case forever. Taking the mean value will not compensate for the overall lower quality of the groups. So, an optimal number of groups can be found.

4.5 Deterioration of reflectance estimations with decreased registration accuracy

A total of 49 simulated VGT images, corresponding to East-West and North-South shifts of -300m, -200m, -100m, 0m, 100m, 200m and 300m, were used to estimate the relative error averaged over the classes to analyse the deterioration of reflectance estimation with decreased registration accuracy for each spectral band. Again, four groups of pixels were selected and ten trials were made. The mean of the estimated values by each of these groups was then computed.

As seen in fig. 4.7, the relative error estimated for a perfect registration (no shift) is generally increased as the shift is increased for all bands, the greatest increase being a little less than 7% for the VGT2 band. Except on the VGT1 band, the greatest gradient is in the North-West - South-East direction, that is in a direction perpendicular to the St.Lawrence River. This is not surprising since the difference in reflectances between water and the other surfaces is greater for the three longer wavelength bands than for the VGT1 band. Also, the general pattern of land use classes is characterized by NW-SE gradients greater than SW-NE ones. Then, for these bands, errors in the estimated reflectances will be more affected by misregistration along this direction than along the other one.

Finally, it can be seen that the relative error does not vary very much for shifts between -100m and 100m and even between -150m to 150m.

It is also possible to analyse the deterioration of the error for each of the land use classes. Table 4.5 shows that the increase is generally less than 3 %, except for the less represented classes on the image which have maximum errors much greater, as expected. The deterioration of the relative error for the "wet lands" class is presented in fig. 4.8, as an example. Again, a strong NW-SE gradient can be noticed.

Table 4.5 Maximum relative error for a shift up to 300 m and relative error corresponding to perfect registration

Land use classes	**Maximal relative error for shift up to 300 m**	**Relative error no shift**	**Difference**
Water	11.1%	8.1%	3.0%
Dry bare soils	9.6%	9.6%	0.0%
Wet bare soils	8.2%	4.8%	3.4%
Pastures, alfalfa and hay	4.4%	4.4%	0.0%
Forested areas	21.1%	21.1%	0.0%
Wet lands	36.5%	6.5%	**30.1%**
Peat bogs with spruces	5.6%	5.2%	0.5%
Peat bogs with alders	22.1%	12.6%	**9.5%**
Herbaceous fallow lands and bushes	11.4%	9.7%	1.7%
Urban areas and roads	15.7%	15.5%	0.2%

In conclusion, it can be considered that if it is possible to locate the image within let us say 150m from the expected location, the error resulting from misregistration would not change very much our estimations.

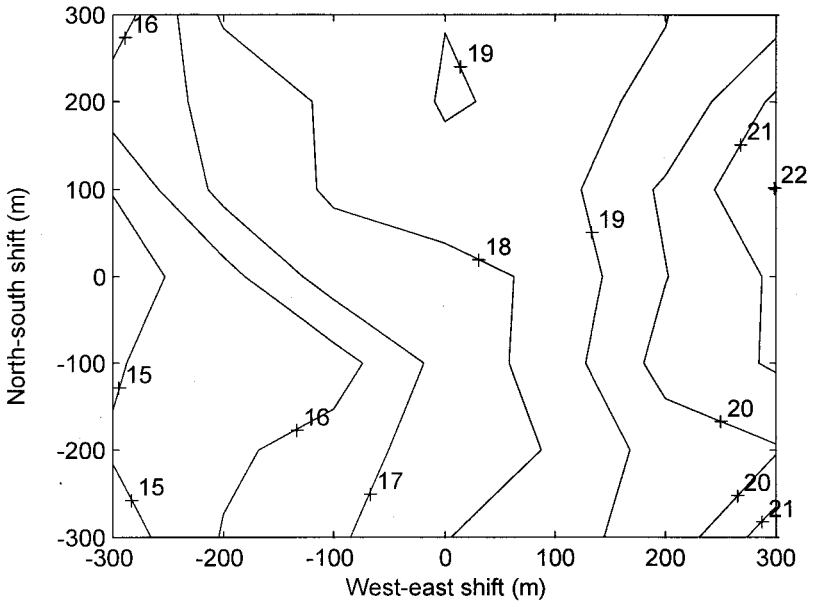

Figure 4.7a

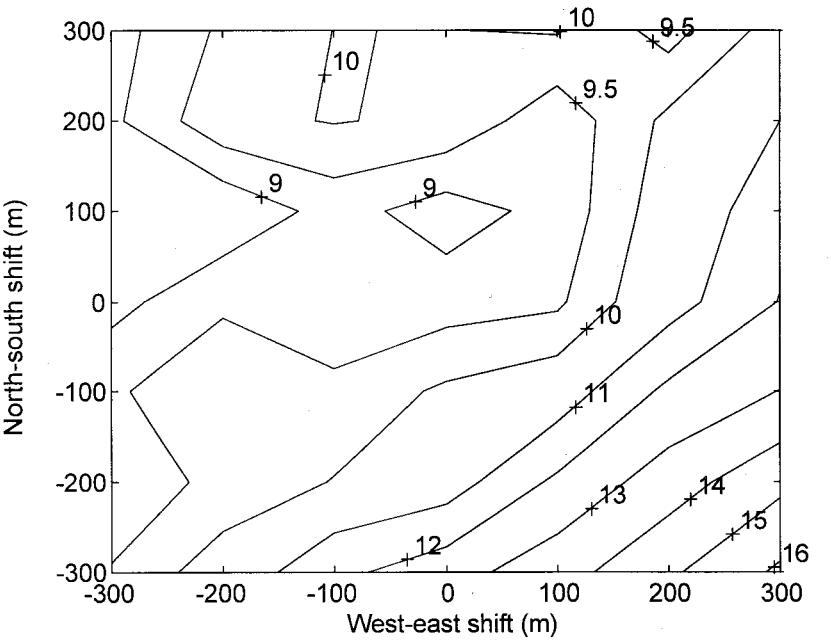

Figure 4.7b

Figure 4.7 Relative error (%) on reflectance estimation for each VGT band as a function of registration accuracy. Mean on land use classes and ten trials. (a) VGT1, (b) VGT2, (c) VGT3, (d) VGT4.

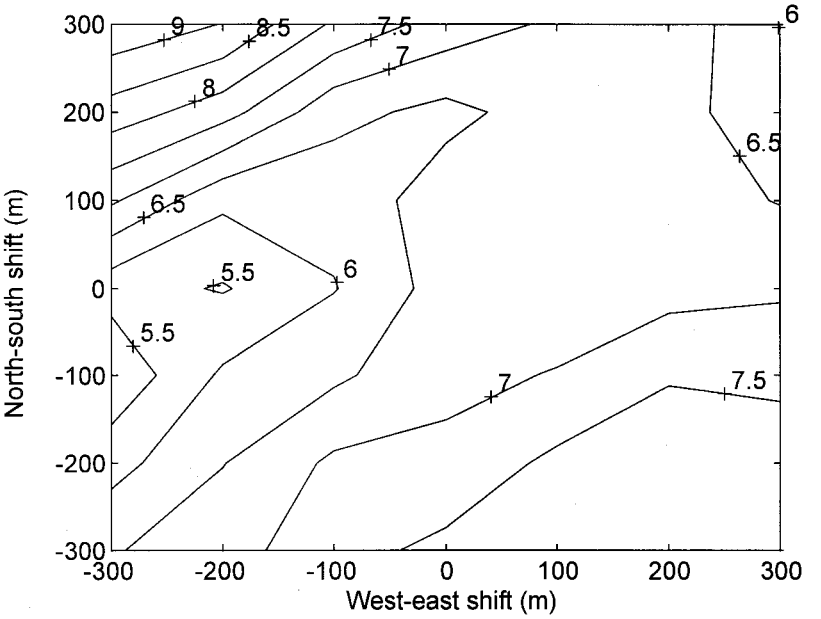

Figure 4.7c

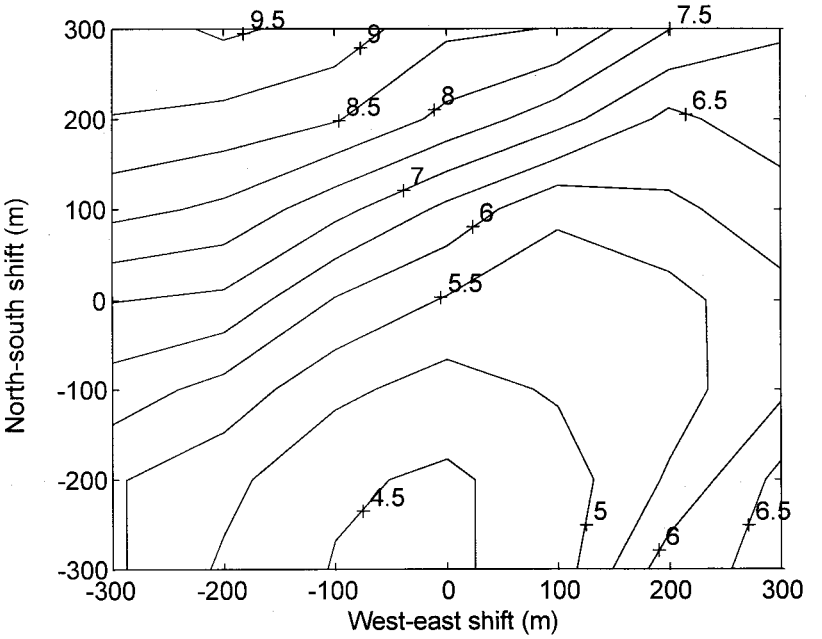

Figure 4.7d

Figure 4.7 (suite) Relative error (%) on reflectance estimation for each VGT band as a function of registration accuracy. Mean on land use classes and ten trials.

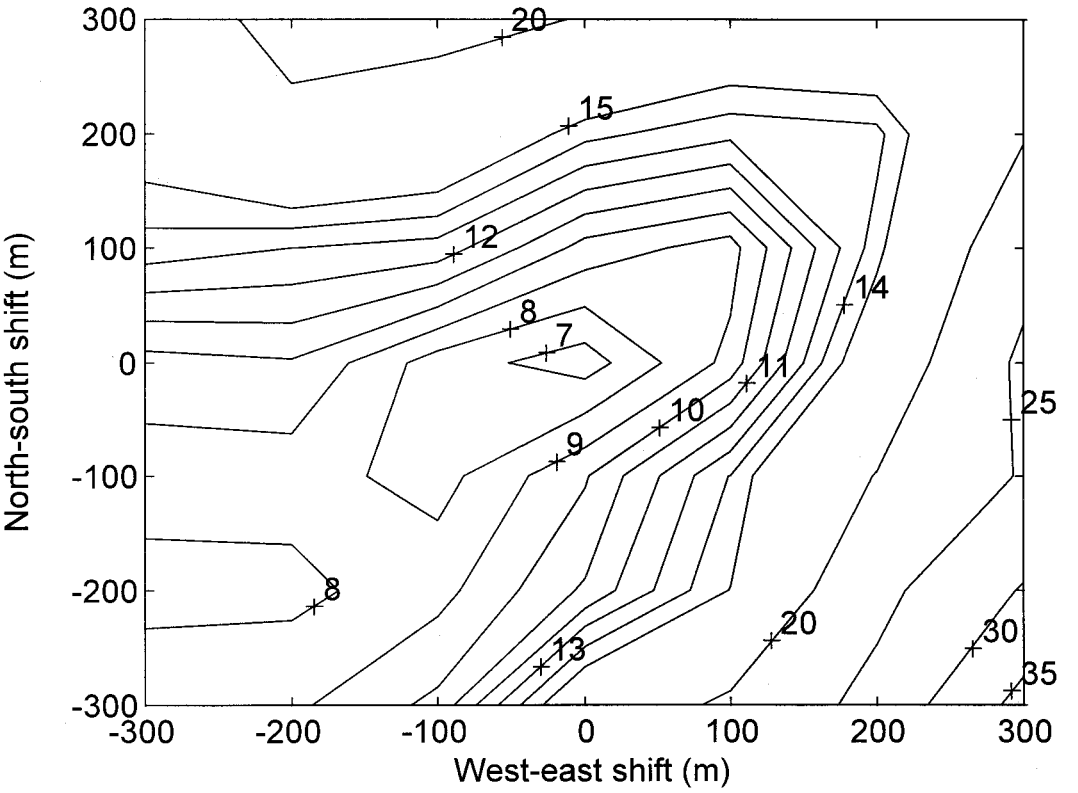

Figure 4.8 Relative error (%) on reflectance estimation as a function of registration accuracy for the small land use class "wet bands". Mean on spectral bands and ten trials.

4.6 Search of optimal location

In an operational context, as explained in section 2.3.2, the exact position of the image is not known, but it is possible to recompute the percentage of occupation of each land use class on each VGT pixel, assuming various shifts. As four groups are used, the location for which the estimated reflectances by each of these four groups are the more similar, should be the seeked location. In practice, we will look for the lowest standard deviation estimated from the values furnished by each of the groups.

A perfect registration has been assumed for the VGT image. Ideally, the lowest standard deviation should then be at (0,0). Let us look at the results on fig. 4.9, for each of the spectral bands.

With the exception of the VGT2 band, a closed polygon corresponding to the lowest standard deviation can be found. For the VGT2 band, the polygon is closed by the limit of the graph. So, in each case, it is possible to estimate, at least approximately, the location of the centers of these polygons. They are, from VGT1 to VGT4, (-30,-25),(-250,-75), (-50,90), (-10,150). We can go one step further and consider that taking the mean of these four values will give a location that could be a good approximation of the true location of the image. The result is (-116,6). If the VGT2 value is rejected, then the result is (-3,72).

In conclusion, it seems possible to locate the individual bands within 100 to 150m from the true location. The accuracy on the mean position of the four bands could be even better. These results are encouraging, but, of course, we will have to check on other images to see if these accuracies can be reproduced. However, as the image was representative of the land use patterns and types that can be found in Southern Quebec, we are confident that its results should be as good with other images. The confirmation of these results will effectively be given in the analysis of the simulated VGT image over Southern Québec, between the St-François and the Chaudière rivers, to be presented in chapter 5.

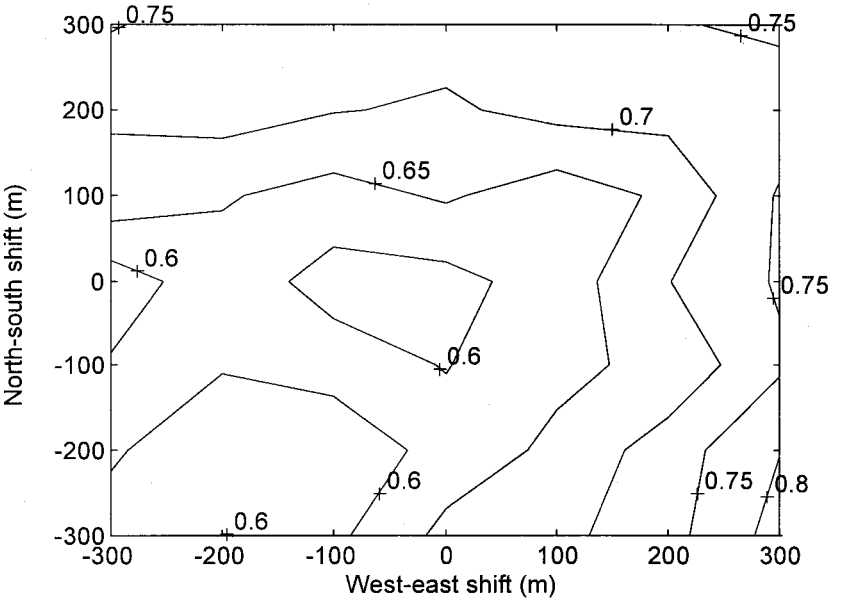

Figure 4.9a VGT1.

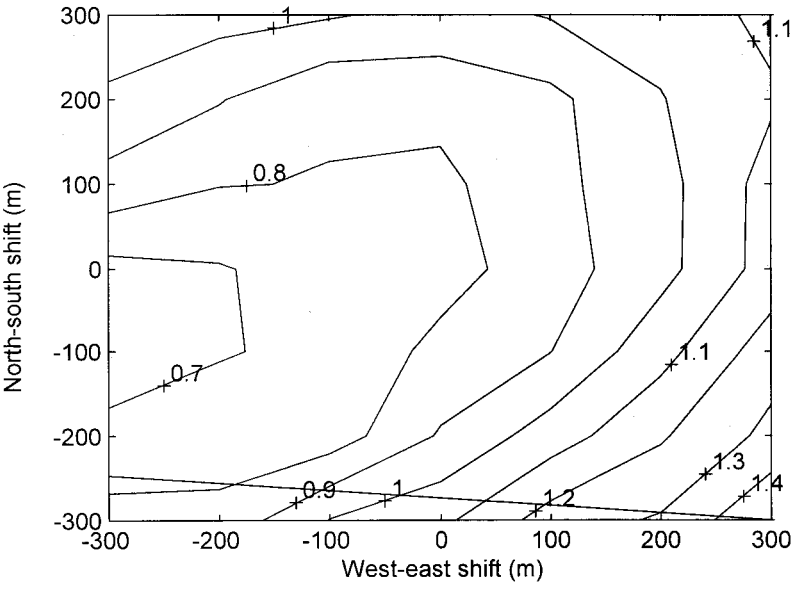

Figure 4.9b VGT2

Figure 4.9 Standard deviation on reflectance estimations as a function of registration accuracy, using four groups of pixels. Mean on land use classes and ten trials.

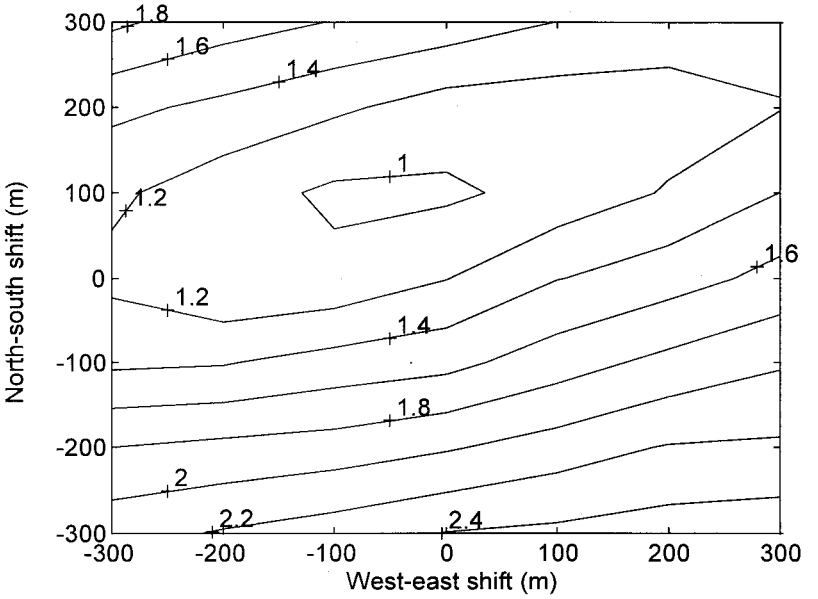

Figure 4.9c VGT3

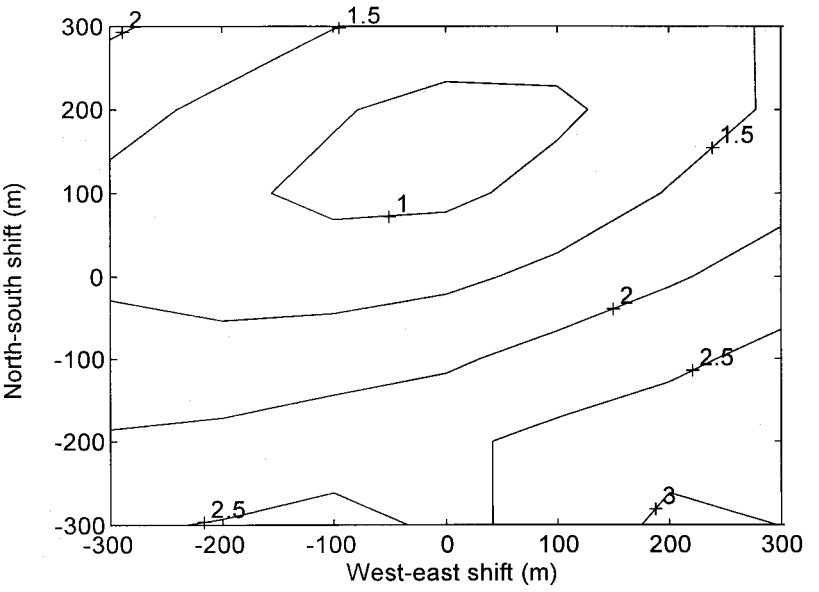

Figure 4.9d VGT4

Figure 4.9 (suite) Standard deviation on reflectance estimations as a function of registration accuracy, using four groups of pixels. Mean on land use classes and ten trials.

5 ESTIMATION OF LAND USE REFLECTANCES FOR SOUTHERN QUEBEC, BETWEEN THE ST-FRANÇOIS AND THE CHAUDIÈRE RIVERS

5.1 Visual evaluation of the simulated HRVIR and VGT images

The original image is a 185km by 185km Landsat TM image of Southern Québec, which has been taken on the 28th of August 1995 at 9:30 a.m. local time. Whereas the image used in chapter 4 was a spring image, this image is a summer one. Prior to any other processing, a 5980 pixels x 5980 lines sub-image the original TM image has been created diminishing the dimensions of the image to 149.5km x 149.5 km. As seen in figure 5.1, the North-West portion of the original image has been kept. The experimental site goes from the Trois-Rivières/Nicolet area in the North-West portion of the image to just South of Québec city in the North-East part. Along the southern limit, we can see, from West to East, the city of Sherbrooke, Mount Megantic and Lake Megantic. Apart from Lake Megantic, we can also notice, to the NNW of this lake, two more lakes, Lake St.François and Lake Aylmer (to the left of the previous one). The St.François river is clearly seen flowing to the SW from Lake Aylmer to the city of Sherbrooke and then to the NW towards the St. Lawrence river. Also, in the Eastern part of the image, the Chaudière river flows in a Northerly direction from Lake Megantic to the St.Lawrence river. The region is characterized by various topographic features from the St. Lawrence Lowlands in the North-West to the Appalachian range in the South-East. Forested as well as agricultural and humid areas, rivers and open-sky mines can also be found. Soils vary within the region, going from marine deposits in the St. Lawrence plain to peat, till and rocky outcrops.

For that summer TM image, we had only the TM3,TM4 and TM5 bands. This means that the HRVIR1 and VGT1 bands were not simulated. Considering our objectives, this is not crucial. Simulation and further processing of the simulated bands have lead to very good results, as will be seen in this chapter.

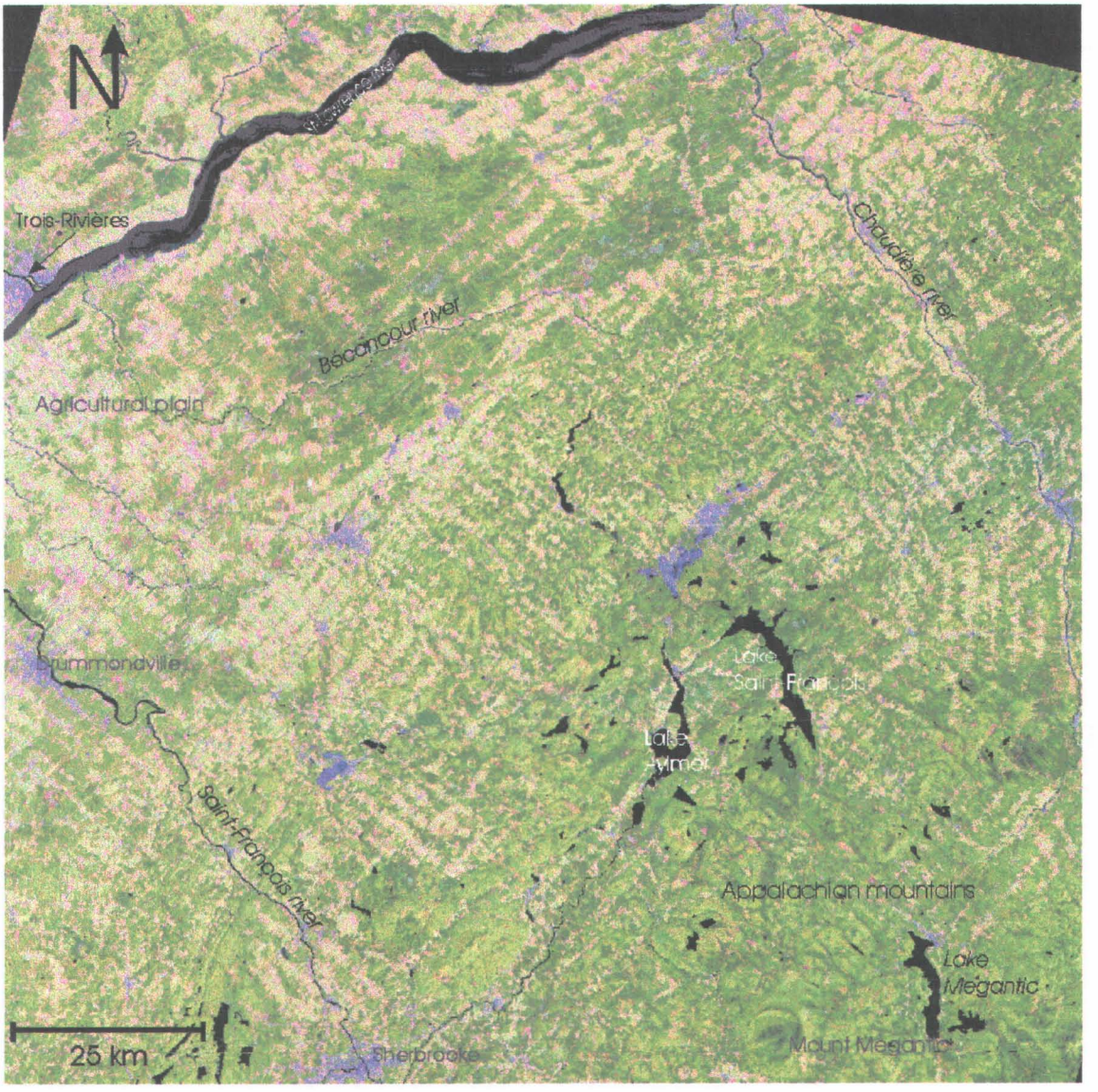

Figure 5.1: Original TM image (TM5, TM4, TM3 - August 28, 1995) for Southern Quebec.

As in the case of the previous image, before simulating the HRVIR and VGT images, atmospheric corrections have been applied to the original image, whose acquisition had been done under ideal cloudless meteorological conditions. As the simulation procedure is the same as that used to simulate the HRVIR and VGT images presented in chapter 4, we will not repeat it here.

The simulated HRVIR2, HRVIR3 and HRVIR4 images are shown in figure 5.2. The Chaudière river has been added to the rivers already seen on the Nicolet image of chapter 4. So, from West to East, we can identify, on the South shore of the St. Lawrence river, the St.Francois, Nicolet (two branches), Bécancour and Chaudière rivers. Of course, these can be seen much easier on the HRVIR4 band. Agricultural areas can also be distinguised from forested areas by their field patterns and higher reflectances, particularly in the HRVIR2 and HRVIR4 bands.

A total of six VGT images have been simulated, in order to verify if the results obtained with the previous image could be obtained with this image, with due care for the possible pre-launch estimated shift of the image relative to the assumed position. The first one corresponds to perfect fit with the HRVIR image. The next four correspond to shifts of (-250m,100m), (250m, -150m), (-50m, -275m), (200m, 200m) for all spectral bands relative to the assumed HRVIR position. Finally, a sixth one corresponds to shifts between spectral bands as well as between those and the assumed exact HRVIR position: (200m, - 200m) for VGT2, (175m,-225m) for VGT3 and (225m, -150m) for VGT4. Those images have been obtained in practice by shifting the mean 46 x46 filter on the original TM image. The VGT images corresponding to the three spectral bands and position (0,0) are presented in figure 5.3. Not much more than for the previous spring VGT images can be said about the features seen on the images. Again, rivers and lakes can be distinguished on the VGT3 and VGT4 images, whereas forested areas are more identified on the VGT2 image than on the other two.

Finally, color composites of bands 2,3 and 4 for both HRVIR and VGT images are shown in figure 5.4. As mentioned for the single- band images, agricultural areas can be distinguished from forested areas. The main lakes and rivers can also be identified on the VGT color composite.

HRVIR2

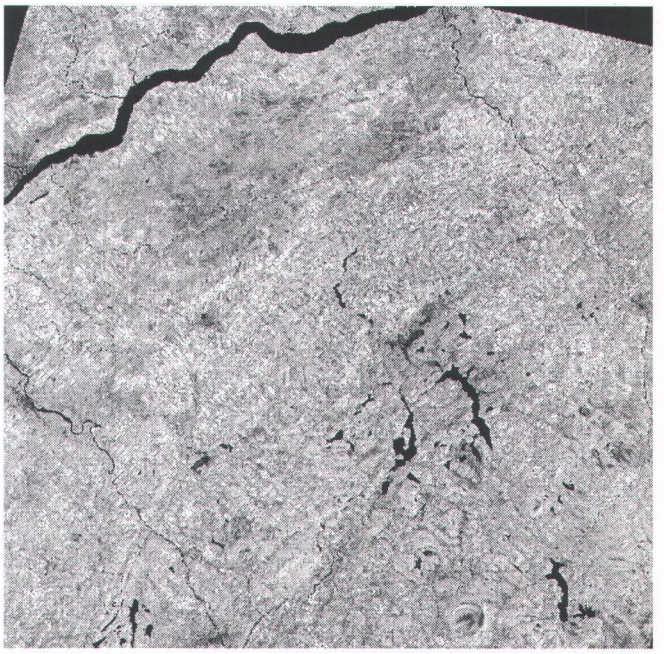

HRVIR3

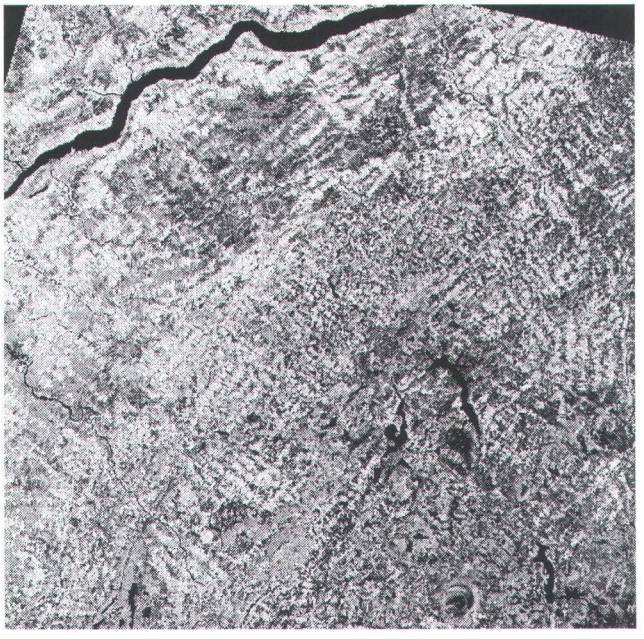

HRVIR4

Figure 5.2 Simulated HRVIR bands - August 28, 1995

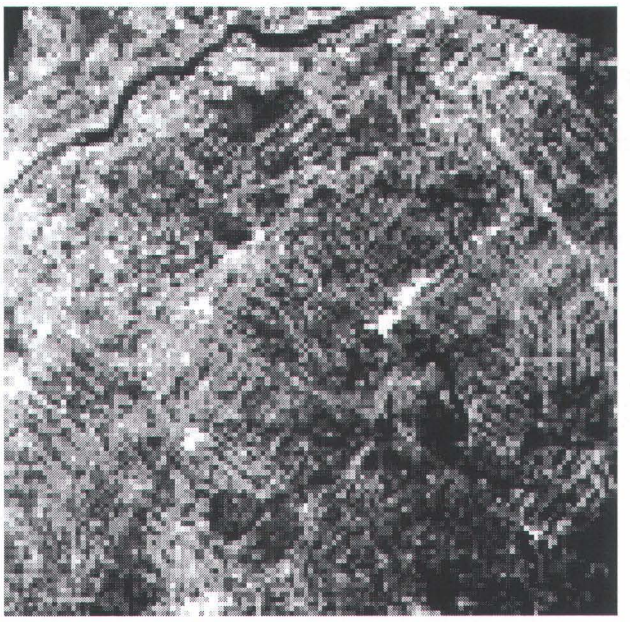

VGT2

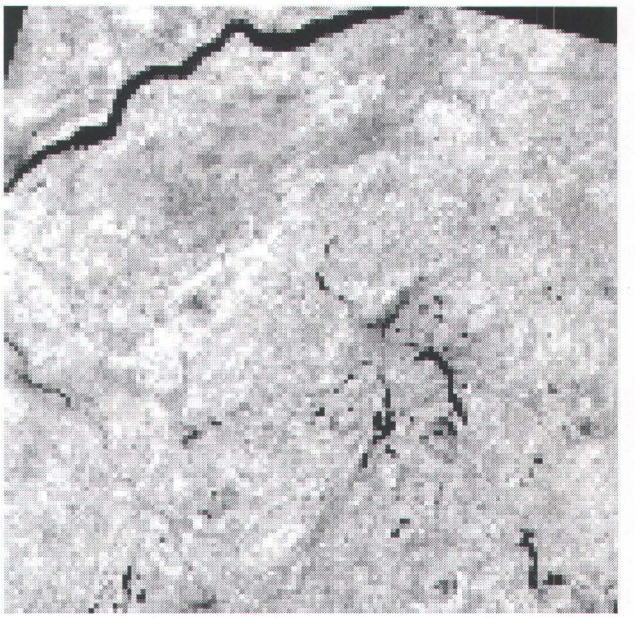

VGT3

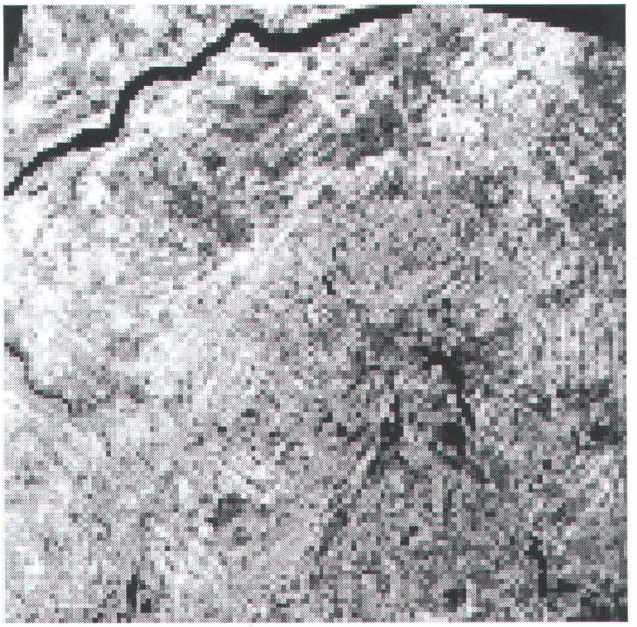

VGT4

Figure 5.3 Simulated VGT bands - August 28, 1995

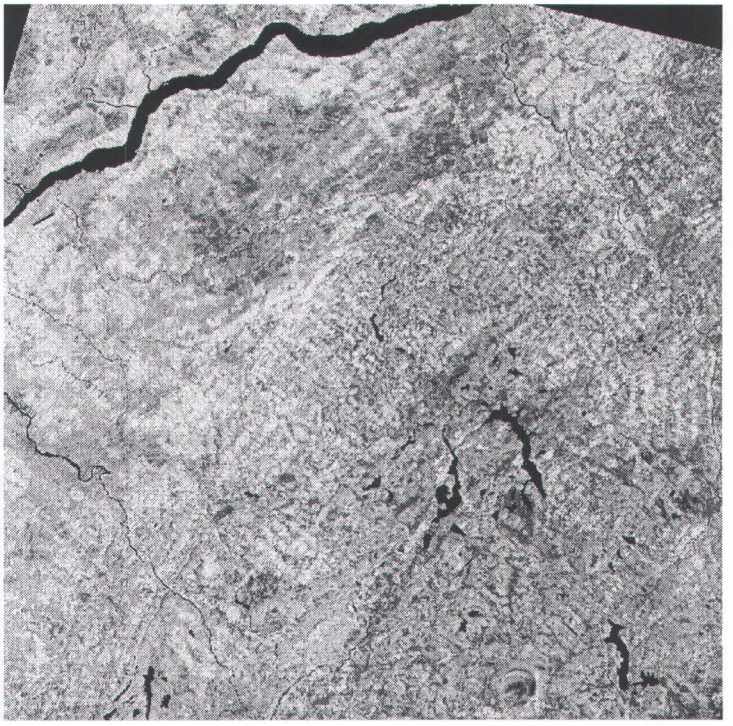

a) HRVIR bands (HRVIR4, HRVIR3, HRVIR2)

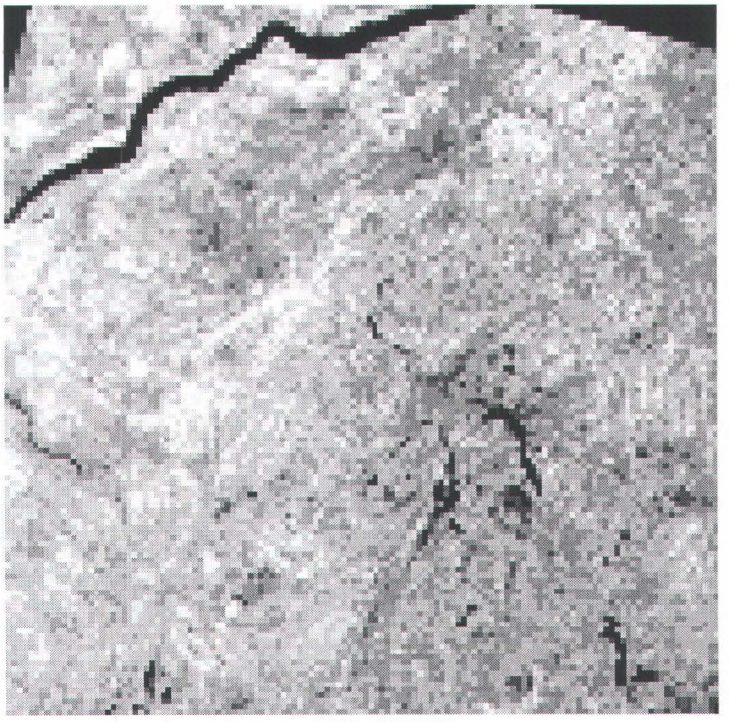

b) VGT bands (VGT4, VGT3, VGT2)

Figure 5.4: Simulated false color composites of HRVIR and VGT bands - August 28, 1995

5.2 Classification results

Again, the Maximum Likelyhood algorithm has been used to prepare a classification of the simulated HRVIR image in order to obtain the percentage of each land use class present in each VGT pixel (figure 5.5). As seen in table 5.1a, a total of ten land use classes have been identified on the image. The percentages of occupation range from 3.9 % for corn to 23.5 % for mixed forest with deciduous species prevailing. It can be seen that the standard deviations for water in bands 3 and 4 are relatively high compared to the mean reflectance, but this is not surprising considering the low reflectances of water in these bands. Otherwise, the standard deviations are relatively normal, knowing the possible variability of reflectance from pixel to pixel for a specific land use class.

Due to limitations in the MATLAB program enabling to find out the most accurate location of the VGT images together with the estimations of reflectances, a 3000 pixels by 2000 lines sub-image of the image appearing on figure 5.5 has been used for that purpose. The statistics of the sub-image have been computed and appear in table 5.1b. In that case, the percentages of occupation range from 1.2 for corn to 32.4 for mixed forest with deciduous species prevailing. Small variations of the reflectance values can be noticed between tables 5.1a and 5.1b, but well below the standard deviations.

5.3 Optimal number of groups for the estimation of class reflectances

It was shown in chapter 4 than an optimal number of groups of pixels could be found to proceed to the estimation of class reflectances. That number was four. It was interesting to verify how many groups would lead to the best estimation in the case of a new image. Again, the procedure for pixel selection and determination of the optimal number of groups is that explained in sections 2.2.4 and 2.2.5.

Table 5.1 Mean reflectance, standard deviation and percentage of occupation for each of the identified land use classes. (a) complete image (b) sub-image used for reflectance and registration accuracy estimation (rectangle in figure 5.5)

A)

Land use classes	% of land use occupation	Reflectance (%)					
		HRVIR2		HRVIR 3		HRVIR 4	
		Mean (%)	Standard Deviation (%)	Mean (%)	Standard Deviation (%)	Mean (%)	Standart Deviation (%)
Out of the image	1,1	--	--	--	--	--	--
Urban areas and roads	5,8	6,9	3,2	27,1	6,3	17,6	4,1
Pastures and alfalfa	14,1	4,4	0,9	44,6	5,7	21,8	2,1
Cereals	5,5	5,4	0,9	37,0	2,5	24,5	7,1
Corn	1,2	4,8	0,4	41,1	2,5	18,9	1,1
Water	2,9	1,8	1,1	1,7	2,6	0,7	1,5
Wet lands	3,0	5,4	1,0	28,6	3,8	17,9	2,2
Bare soils	5,0	9,2	3,5	31,1	5,2	26,8	3,5
Herbacious fallow landsand bushes	16,2	3,3	0,9	32,7	3,3	17,7	2,5
Mixed forest (mostly deciduous)	32,4	2,2	0,4	35,4	5,1	15,0	2,5
Coniferous forest	13,4	2,0	0,5	24,3	3,1	9,9	1,6

B)

Land use classes	% of land use occupation	Reflectance (%)					
		HRVIR2		HRVIR 3		HRVIR 4	
		Mean (%)	Standard Deviation (%)	Mean (%)	Standard Deviation (%)	Mean (%)	Standart Deviation (%)
Out of the image	0	0	0	0	0	0	0
Urban areas and roads	4,6	7,4	3,1	27,2	6,5	18,3	4,3
Pastures and alfalfa	14,56	4,6	0,9	45,0	5,8	21,9	2,0
Cereals	8,8	5,5	0,9	36,9	2,5	24,8	1,9
Corn	3,9	4,8	0,4	42,1	2,4	19,2	1,0
Water	3,9	2,7	0,7	2,7	3,4	0,7	1,5
Wet lands	6,0	5,4	1,0	28,7	3,7	18,2	2,1
Bare soils	8,6	9,6	3,2	31,2	5,0	27,1	3,4
Herbacious fallow landsand bushes	15,9	3,3	0,9	32,7	3,1	17,5	2,2
Mixed forest (mostly deciduous)	23,5	2,3	0,4	34,6	4,1	14,9	2,0
Coniferous forest	10,4	2,3	0,4	24,6	2,8	10,4	1,5

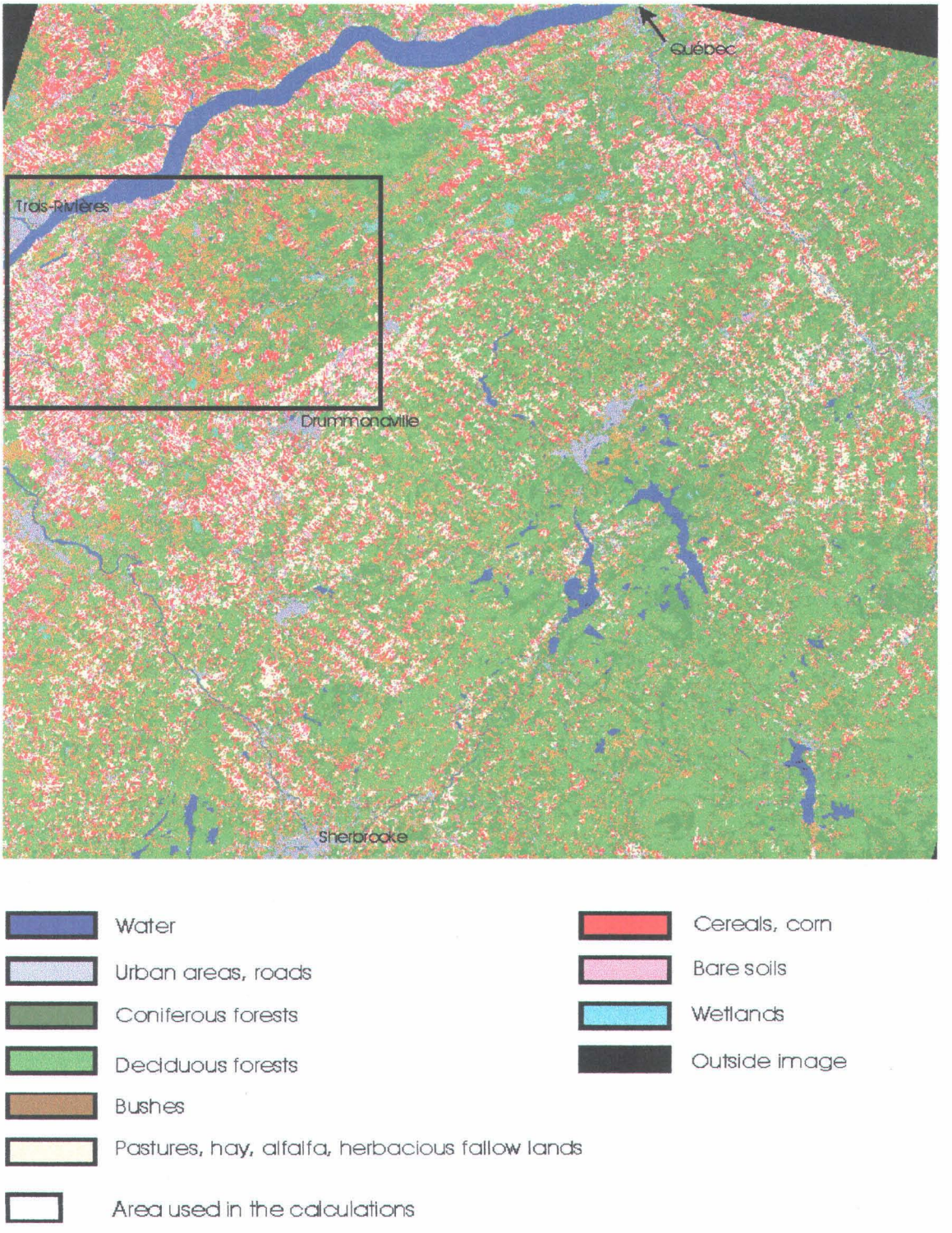

Figure 5.5: Classified HRVIR image - August 28, 1995

The variation of the relative error (%) as the number of groups is increased is presented in figure 5.6. It can be seen that, in agreement with the results presented in figure 4.5, the relative error is lowest when the number of groups is increased to four (4) in bands 2 and 4. This not the case in band three (3), but there is not much variation between 3 and 10 groups, in that case. If the land use class "water" is excluded from the computation, the mean relative error considering all three bands together is 4, . It can also be noticed that a larger number of groups would not deteriorate the error very much. More precise values of the relative errors (%) for one and four groups are also presented in table 5.2.

As there were no reasons to change the number of groups for the estimations of the reflectances of the land use classes from the VGT images, we kept the optimal number of groups to four.

5.4 Determination of the actual position of a VGT image relative to the expected position

Let us recall here that in an operational context, the exact position of a specific VGT image is not known, but that it is possible to recompute the percentages of occupation of each land use class on each VGT pixel, assuming various shifts. Again, as four groups of pixels are used, the position for which the estimated reflectances by each of these four groups are the more similar should be the seeked position. In practice, we will look for the lowest standard deviation estimated from the values furnished by each of the groups.

In the present case, two methods of estimation have been used: detailed standard deviation mapping and heuristic search.

5.4.1 Detailed standard deviation mapping.

As previouly, a maximum shift of 300 m has been assumed in each direction, defining a seach area of 600m x 600m centered on the expected true position. In order to map the variation of the standard error with position within the search area, the latter has to be computed using a grid size sufficiently small. In the present case, a grid size of 50 m has been selected, giving 169 values from

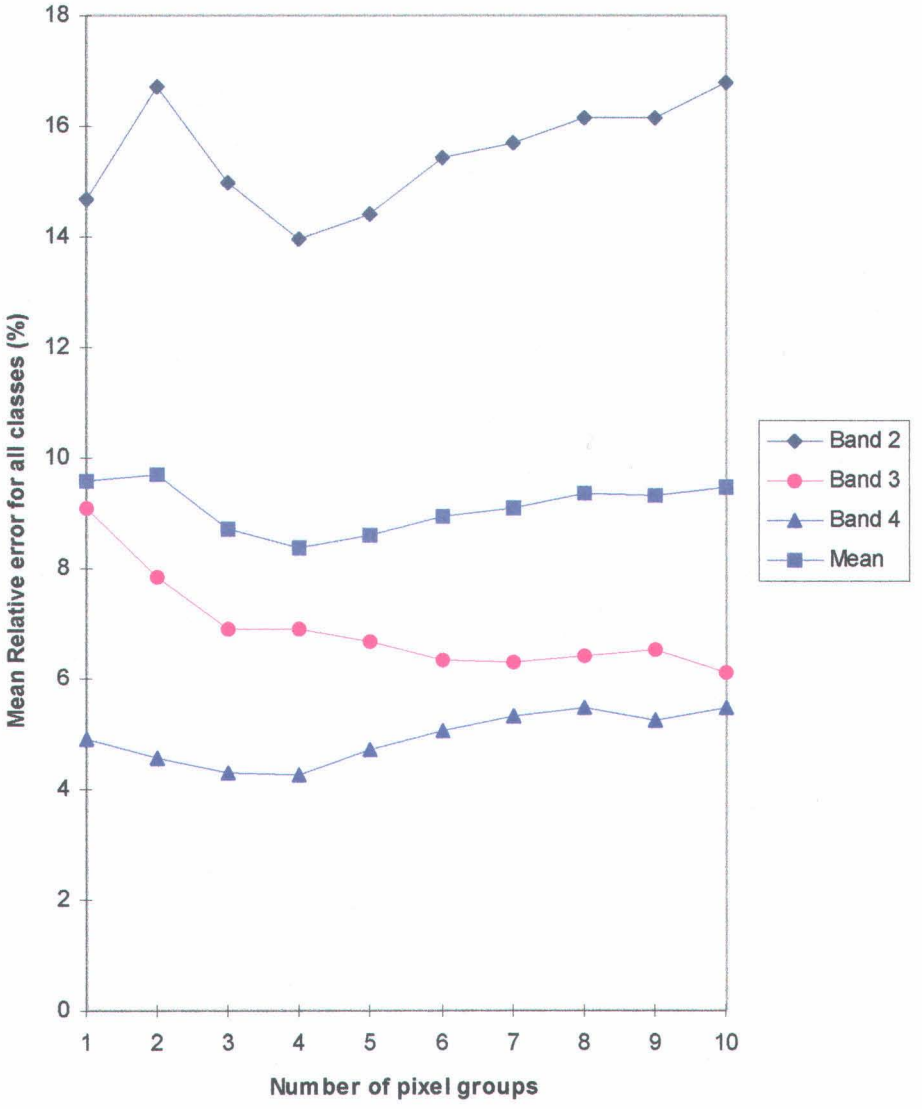

Figure 5.6: Relative error (%) for each VGT band, as a function of the number of pixel groups. Mean on classes excluding the "water" class

Table 5.2 Relative error (%) for each land use class, using 1 and 4 groups of pixels. Mean value of ten trials using 10 best pixels, plus 10 random pixels

CLASSES	VGT2		VGT3		VGT4	
	1 group	4 groups	1 group	4 groups	1 group	4 groups
Urban areas and roads	49,4	39,3	33,52	23,0	11,1	5,9
Pastures and alfalfa	12,3	5,6	10,04	9,8	1,4	2,0
Cereals	2,0	2,3	7,48	4,0	1,8	3,9
Corn	5,4	4,5	1,61	1,4	5,3	3,2
Water	30,3	21,4	18,40	63,9	95,6	97,7
Wet lands	14,3	16,5	11,02	2,8	0,8	4,1
Bare soils	3,1	2,1	3,84	4,3	6,3	4,1
Herbacious fallow landsand bushes	11,6	15,0	37	1,9	1,7	1,7
Mixed forest (mostly deciduous)	17,3	14,9	444	3,2	1,9	1,9
Coniferous forest	16,9	25,6	9,63	11,8	14,0	14,0
Mean on classes (excluding water)	14,7	14,0	9,11	6,9	4,9	4,5

which a map could be drawn. This exhaustive computation was performed for each of the 6 simulated VGT images and the resulting maps are shown in appendix A. It can be seen readily that most of the maps have relatively smooth gradients, allowing a slow degradation of the results as the distance between the estimated position and the "true" position increases. This means that a perfect fit between the VGT image and the classified HRVIR image is not a must within certain limits, as found out in the preceeding chapter for the first image.

The subjectively estimated positions from the standard deviation maps for the six simulated VGT images are presented in table 5.3. It can be noticed that for any of the "true shifts", the estimated shift is normally well below 100m, and as low as 10m for shift no. 3, when the mean of the shifts with regards to the individual bands is computed. But, even for individual bands, most of the distances between the estimated and "true" positions are well below 100m. In particular, for the last image, for which each of the band is taking a different "true" position, the distances are respectively 25, 25 and 46m, which is an excellent result.

It thus seems quite clear that the developed methodology allows determination of the "true" position of the portion of a VGT image of interest for a specific region with an accuracy of better than 100m.

5.4.2 Heuristic search

As mentioned in section 2.3.2, it is also possible to use an heuristic hill-climbing procedure to find out the "true position" of a VGT image. The search was done according to the procedure outline in that section and the results are shown in table 5.4. The mean distances between the "true positions" and the estimated positions are larger than with the detailed mapping of the standard deviation values, but still acceptable, the smallest distance being 27m and the largest 153m. One should remember that the gradients are often low in the vicinity of the "true position" so that trying to find an optimal position with that type of gradients can easily lead to the estimations discussed above.

Table 5.3 Estimated X-Y shifts of the VGT2, VGT3 and VGT4 bands as compared to the actual simulated shifts with respect to the HRVIR image. Values estimated from detailed standard deviation mapping

VGT image 1 (no shift: X=0 m, Y=0 m)

	VGT2	VGT3	VGT4	Average
Estimated shift in X (m)	0	0	-65	22
Estimated shift in Y (m)	-100	-75	-150	92
Distance from the simulated location (m)	100	75	119	96

VGT image 2 (Simulated shift: X=-250 m, Y=100 m)

	VGT2	VGT3	VGT4	Average
Estimated shift in X (m)	-230	-250	-210	-230
Estimated shift in Y (m)	50	80	35	55
Distance from the simulated location (m)	54	20	76	49

VGT image 3 (Simulated shift: X=250 m, Y= -150 m)

	VGT2	VGT3	VGT4	Average
Estimated shift in X (m)	250	240	175	222
Estimated shift in Y (m)	-235	-185	-150	-190
Distance from the simulated location (m)	85	36	75	48

VGT image 4 (Simulated shift: X=-50 m, Y= -275 m)

	VGT2	VGT3	VGT4	Average
Estimated shift in X (m)	-110	-20	-25	-52
Estimated shift in Y (m)	-280	-230	-285	-265
Distance from the simulated location (m)	60	54	27	10

VGT image 5 (Simulated shift: X=200 m, Y=200 m)

	VGT2	VGT3	VGT4	Average
Estimated shift in X (m)	225	85	245	185
Estimated shift in Y (m)	215	105	225	182
Distance from the simulated location (m)	29	149	51	23

VGT image 6 (Simulated shift: VGT2: X=200 m, Y=-200 m; VGT3: X=175 m, Y=-225 m; VGT4: X=225 m, Y=-150 m)

	VGT2	VGT3	VGT4	Average
Estimated shift in X (m)	225	150	170	--
Estimated shift in Y (m)	-195	-230	-160	--
Distance from the simulated location (m)	25	25	46	--

Table 5.4 Estimated X-Y shifts of the VGT2, VGT3 and VGT4 bands as compared to the actual simulated shifts with respect to the HRVIR image. Values estimated from heuristic research algorithm

VGT image 1 (no shift: X=0 m, Y=0 m)

	VGT2	VGT3	VGT4	Average
Estimated shift in X (m)	0	0	0	0
Estimated shift in Y (m)	-20	-60	0	-27
Distance from the simulated location (m)	20	60	0	27

VGT image 2 (Simulated shift: X=-250 m, Y=100 m)

	VGT2	VGT3	VGT4	Average
Estimated shift in X (m)	-200	-180	-200	-193
Estimated shift in Y (m)	160	160	180	167
Distance from the simulated location (m)	78	92	94	88

VGT image 3 (Simulated shift: X=250 m, Y=-150 m)

	VGT2	VGT3	VGT4	Average
Estimated shift in X (m)	160	160	140	153
Estimated shift in Y (m)	-160	-160	-160	-160
Distance from the simulated location (m)	91	91	110	98

VGT image 4- Trial 1 (Simulated shift: X=-50 m, Y=-275 m)

	VGT2	VGT3	VGT4	Average
Estimated shift in X (m)	-160	180	0	7
Estimated shift in Y (m)	-200	-180	-20	-133
Distance from the simulated location (m)	133	249	260	153

VGT image 4- Trial 2 (Simulated shift: X=-50 m, Y=-275 m)

	VGT2	VGT3	VGT4	Average
Estimated shift in X (m)	-160	-160	-100	-140
Estimated shift in Y (m)	-200	-120	-160	-160
Distance from the simulated location (m)	133	190	125	146

Tableau 5.4 (cont.)

VGT image 5- Trial 1 (Simulated shift: X=200 m, Y=200 m)

	VGT2	VGT3	VGT4	Average
Estimated shift in X (m)	-20	160	160	100
Estimated shift in Y (m)	40	180	160	127
Distance from the simulated location (m)	133	45	57	124

VGT image 5- Trial 2 (Simulated shift: X=200 m, Y=200 m)

	VGT2	VGT3	VGT4	Average
Estimated shift in X (m)	180	180	160	173
Estimated shift in Y (m)	200	160	180	180
Distance from the simulated location (m)	20	45	45	34

VGT image 6 (Simulated shift: VGT2: X=200 m, Y=-200 m; VGT3: X=175 m, Y=-225 m; VGT4: X=225 m, Y=-150 m)

	VGT2	VGT3	VGT4	Moyenne
Estimated shift in X (m)	140	160	160	153
Estimated shift in Y (m)	-160	-160	-200	-173
Distance from the simulated location (m)	72	67	82	74

5.4.3 Comparison of the two approaches

The positions estimated by each of the two approaches are compared to the "true shifts" in figure 5.7. It can be seen rapidly that none of the approaches is systematically more accurate than the other, but that both methods give generally good results. Again, as the estimation of the reflectances does not vary very much as long as the distance between the estimated position and the "true position" is smaller than approximately 100m, the achieved location accuracy is quite satisfactory as it will be shown in the next section.

5.5 Accuracy of estimated reflectances

Knowing that it is possible to locate the VGT images with a very good accuracy, it remains to verify if the mean reflectances of the various land use classes can be estimated also with a very good accuracy. The answer is yes. The reflectances estimated from the VGT images for each of the land use classes and for each spectral band are presented in table 5.5 and in Figure 5.8. It can be noticed that no matter the method to position the image, most of the resulting reflectances are very close to the mean reflectances estimated from the HRVIR image. Also, the accuracy increases from VGT2 to VGT4.

The above results show clearly that it is possible, on an operational basis, to monitor the variation of the reflectances of the land use classes present in a specific region, provided that their percentages of occupation are known.

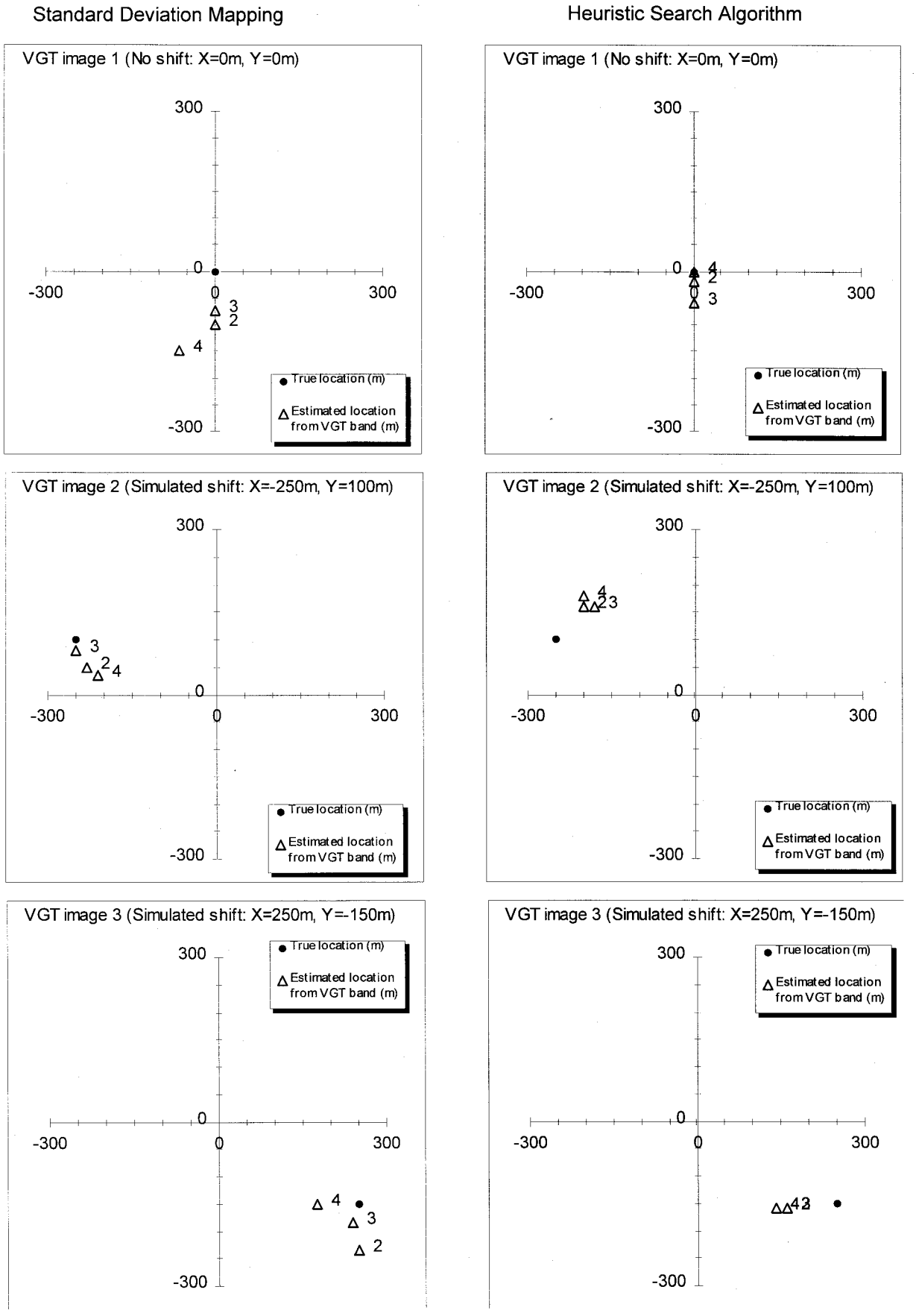

Figure 5.7 Comparison of estimated location for each VGT band using either Standard Deviation Mapping or Heuristic Search. The true location is also shown.

Standard Deviation Mapping

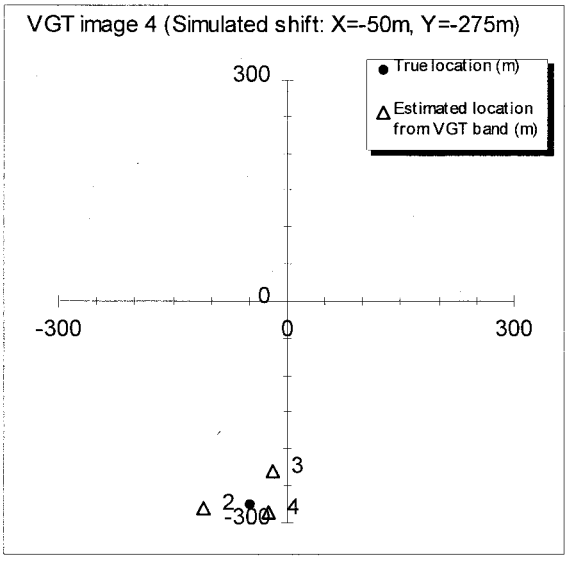

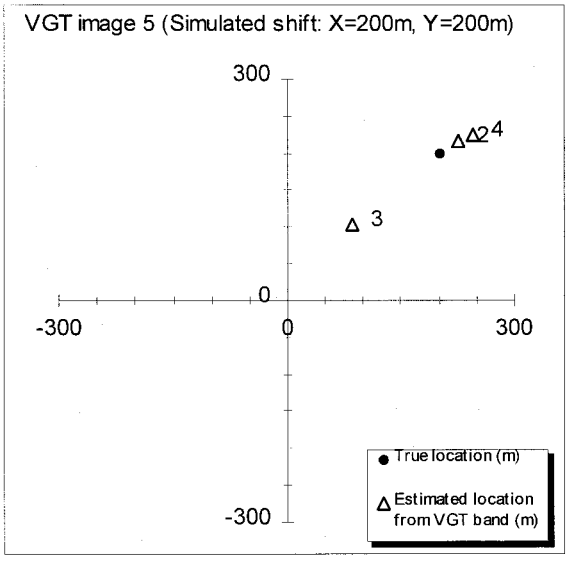

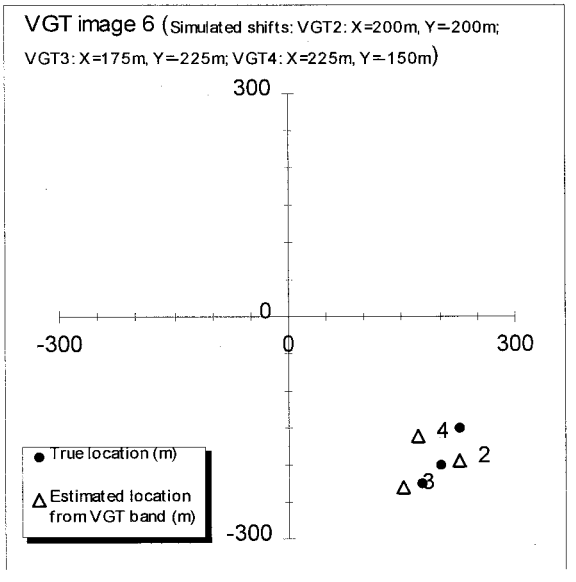

Heuristic Search Algorithm

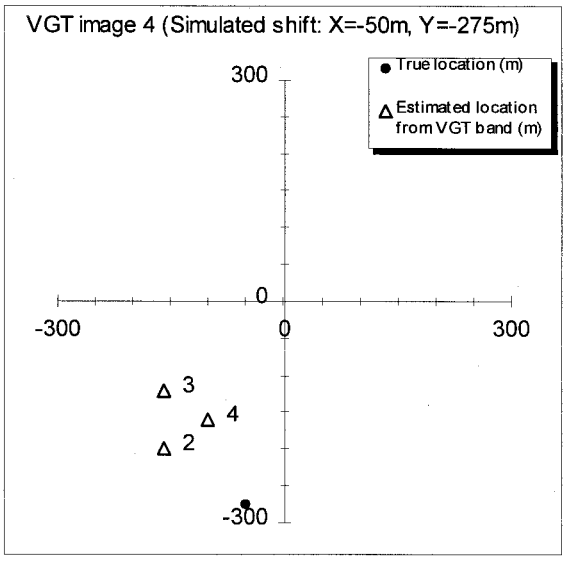

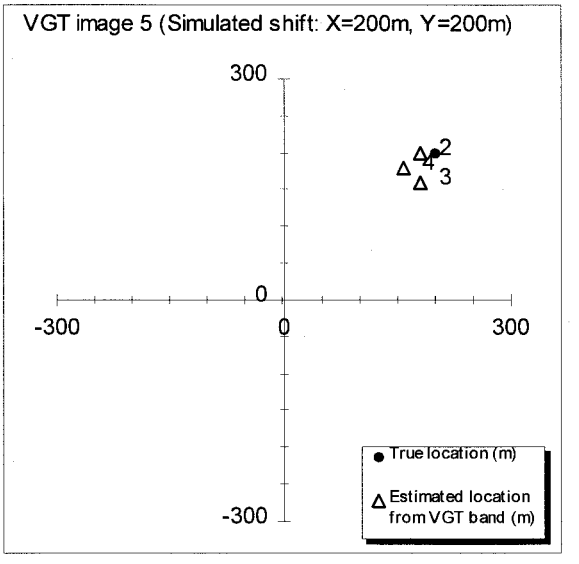

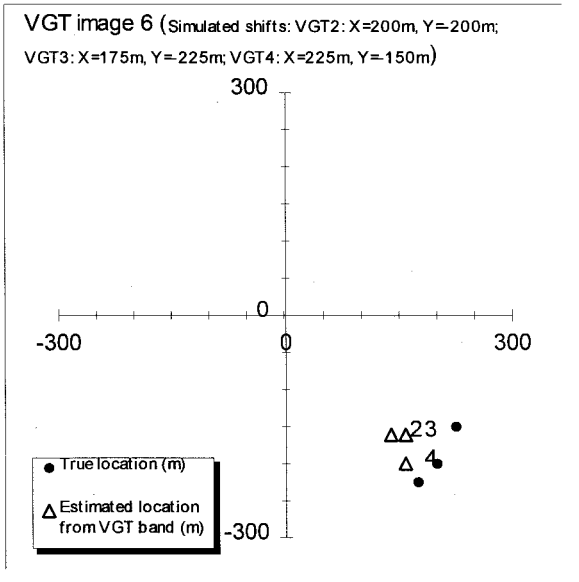

figure 5.7 (cont.)

Table 5.5 Estimated land use reflectances from the VGT spectral lands vs HRVIR reflectances, at location (0,0)

VGT-2 Band

		Estimated reflectances from VGT	
Land use classes	HRVIR Reflectances	Standard error mapping	Heuristic Research
Urban areas and roads	7.36	10.3	10.29
Pastures and alfalfa	4.62	4.35	4.32
Cereals	5.52	5.41	5.4
Corn	4.79	5.15	5
Water	2.73	2.08	2.02
Wet lands	5.43	4.45	4.48
Bare soils	9.61	9.74	9.68
Herbacious fallow lands and hushes	3.28	2.8	2.74
Mixed forest	2.38	2.01	2
Coniferous forests	2.28	1.77	1.79

VGT-3 Band

		Estimated reflectances from VGT	
Land use classes	HRVIR Reflectances	Standard error mapping	Heuristic Research
Urban areas and roads	27.18	21.16	20.86
Pastures and alfalfa	44.99	49.17	49.24
Cereals	36.86	35.69	35.38
Corn	42.07	43.45	42.69
Water	2.7	1.19	1.56
Wet lands	28.72	27.73	28.01
Bare soils	31.23	29.48	29.89
Herbacious fallow lands and hushes	32.66	32.5	31.94
Mixed forest	34.61	35.61	35.8
Coniferous forests	24.61	21.64	21.68

VGT-4 Band

		Estimated reflectances from VGT	
Land use classes	HRVIR Reflectances	Standard error mapping	Heuristic Research
Urban areas and roads	18.34	17.48	17.25
Pastures and alfalfa	21.87	22.16	22.21
Cereals	24.75	25.73	25.79
Corn	19.2	19.18	18.79
Water	0.71	0.07	0.06
Wet lands	18.15	17.4	17.44
Bare soils	27.06	27.9	28.05
Herbacious fallow lands and hushes	17.53	17.5	17.3
Mixed forest	14.87	14.88	15.04
Coniferous forests	10.4	9.09	8.93

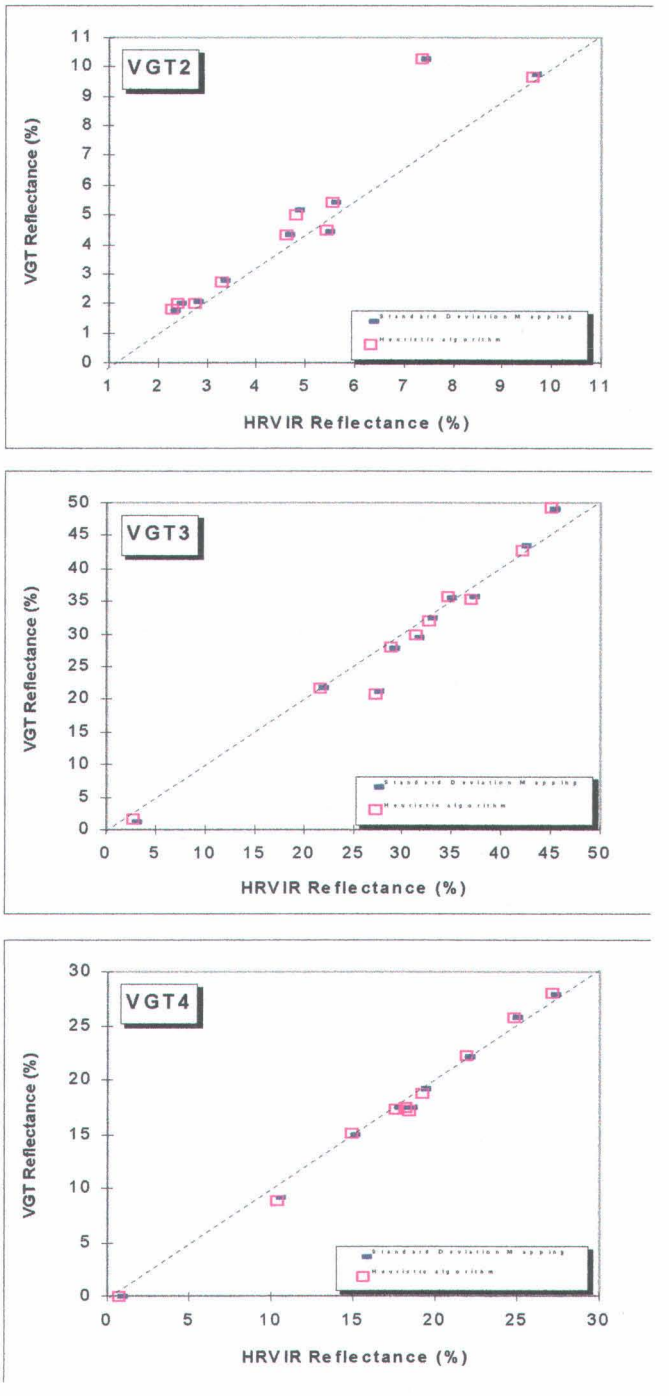

Figure 5.8: VGT estimated reflectances VS HRVIR reflectances

6 ESTIMATION OF THE PERCENTAGE OF SNOW COVER ON EACH VGT PIXEL, FOR THE ST.FRANÇOIS WATERSHED

6.1 Visual evaluation of the simulated HRVIR and VGT images

The original TM image for partial snow cover over the southern portion of the St. François watershed (fig. 6.1) was taken on the 3rd of April 1988 at 9:30 a.m. local time. It corresponds to a quarter of a full TM image.

The St. François river is clearly seen, in the North-West corner of the image, flowing to the SE down to the city of Sherbrooke and then to the North-East toward lake Aylmer (which could be seen on fig. 5.1). To the South-West of the image, lake Magog is mostly frozen, whereas lake Massawipi is unfrozen. The characteristic rounded shape of mount Mégantic can be clearly identified along the easthern border of the image. Snow free areas, mostly in the South-West part of the image, appear in yellow to reddish colors, whereas snow covered areas appear in blue. Green patches appearing mostly in snow covered areas correspond to coniferous forests.

All TM bands were available so that the four HRVIR and VGT bands have been simulated. As for the previous images, atmospheric corrections have been applied to the original image, whose acquisition had been done under cloudless meteorological conditions. Again, as the simulation procedure is the same as that used before, it will not be repeated here.

The simulated HRVIR bands are presented in figure 6.2. Their general appearances are quite different from those in figure 5.2, which corresponds to summer. Snow reflectance in the first three bands is noticeable, particularly for the HRVIR1 and HRVIR2 bands. On the contrary, the pixels with lighter shades of grey in the first three bands have very dark shades of grey in the HRVIR4 band, because of snow absorption at that wavelenght. It is now easier to identify the river network on the HRVIR3 than on the HRVIR4 band, again because of snow absorption.

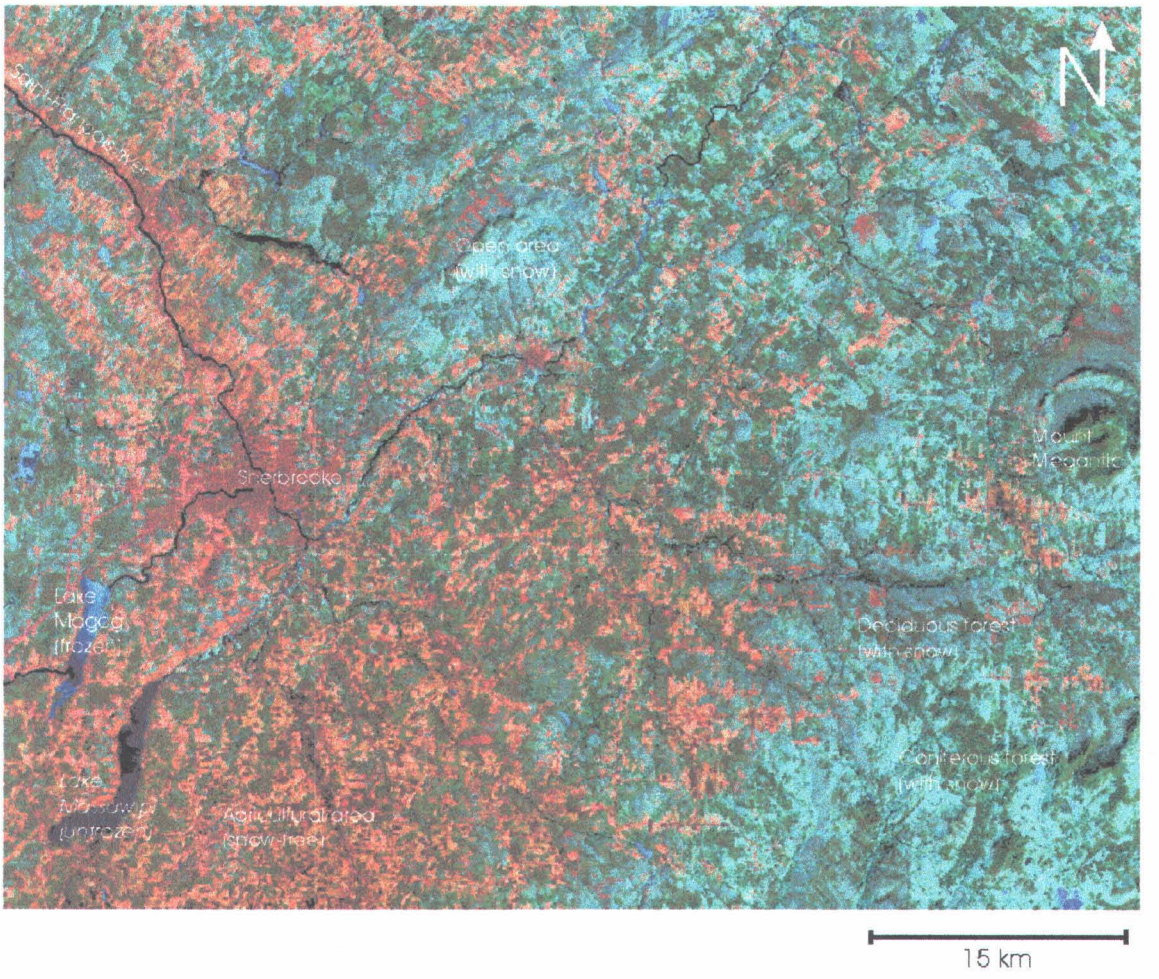

Figure 6.1: Original TM image (TM5, TM4, TM3 - April 2, 1988) for the Saint-François Watershed

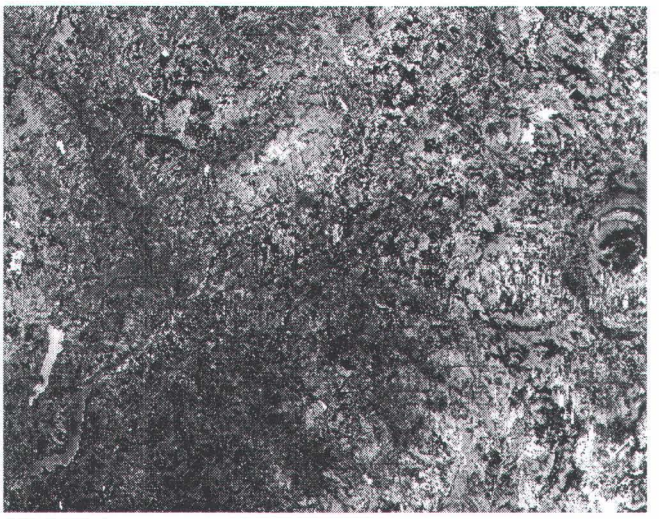

HRVIR1

HRVIR2

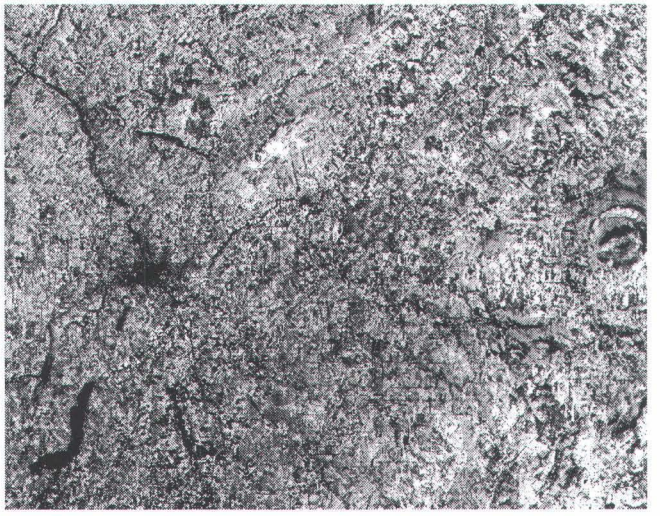

HRVIR3

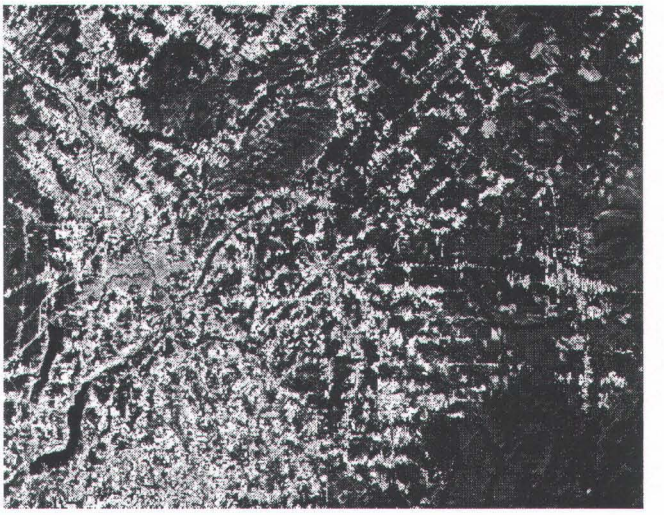

HRVIR4

Figure 6.2 Simulated HRVIR bands - April 2, 1988

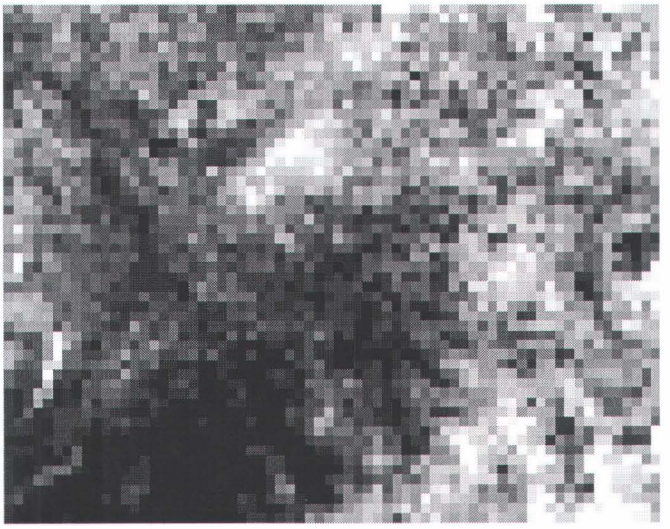

VGT1

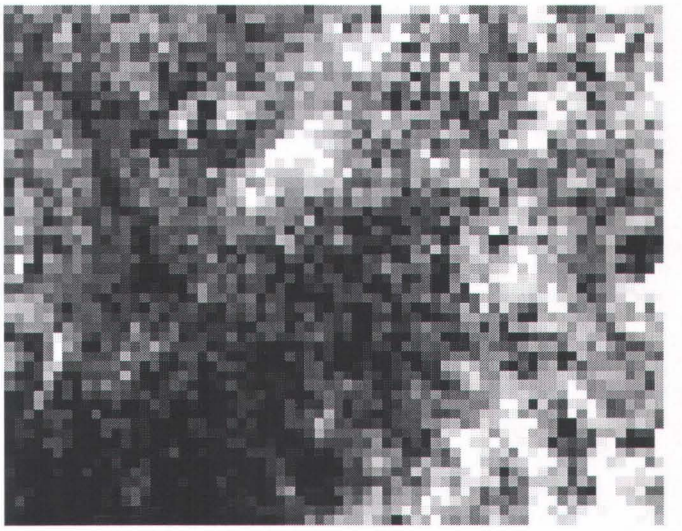

VGT2

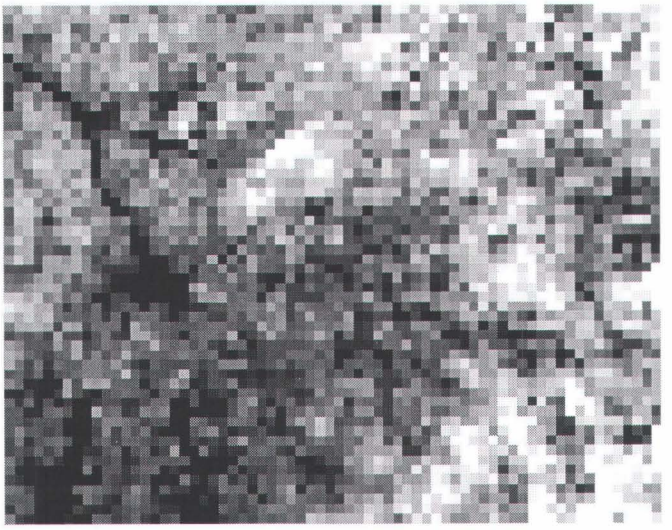

VGT3

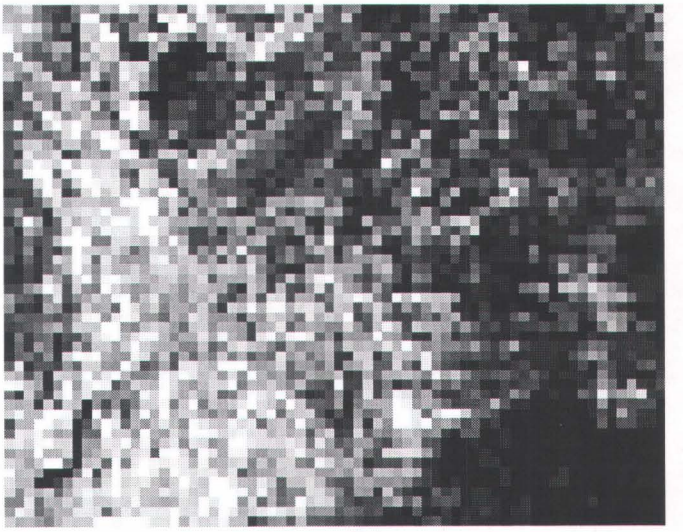

VGT4

Figure 6.3 Simulated VGT bands - April 2, 1988

As it was shown in the previous chapters that it was possible to locate the VGT images normally with an accuracy of better than 100m, the emphasis was put essentially on the information that could be obtained from VGT images, assuming that it was possible to locate them with an acceptable accuracy. The simulated VGT image is thus assumed perfectly fitted to the HRVIR image for that particular application. The four VGT bands are presented in figure 6.3. The St. François river can still be identified on the first three bands, but not on the VGT4 band. On the other hand, it is easier to identify lakes Magog and Massawipi on the VGT4 band than on the other bands. Also, as for the HRVIR bands, the reflectance of snow is quite noticeable on the first three bands, whereas absorption by snow characterizes the VGT4 band.

Color composites of bands 2, 3 and 4 for both HRVIR and VGT images are shown in figure 6.4. For the HRVIR color image, the same details as described for the original TM image can be noticed. On the VGT image, again, the St.François river can be identified in the North-West portion of the image, together with the two lakes in the South-West portion. Also, snow free areas are quite distinguishable from snow covered areas. Pixels that have not a full snow cover appear in colors that are between those characterizing either snow free and snow covered areas.

6.2 Classification results

As with the previous images, the Maximum Likelyhood algorithm has been used to prepare a classification of the simulated HRVIR image in order to obtain the percentage of each land use class present in each VGT pixel (figure 6.5). As seen in figure 6.5 and table 6.1, seven classes were selected on the image: frozen and unfrozen water surfaces, snow covered and snow free open areas, snow covered and snow free deciduous forests and snow covered coniferous forests. It was impossible to clearly identify snow free coniferous forests. Water surfaces occupy less than 3% of the area, whereas open areas occupy 43.5%, of which 19.1% are covered by snow. Deciduous forests occupy 26.8%, of which 21.1% are covered by snow, and, finally coniferous forests occupy 27.1% of the image and are completely covered by snow, according to the classification.

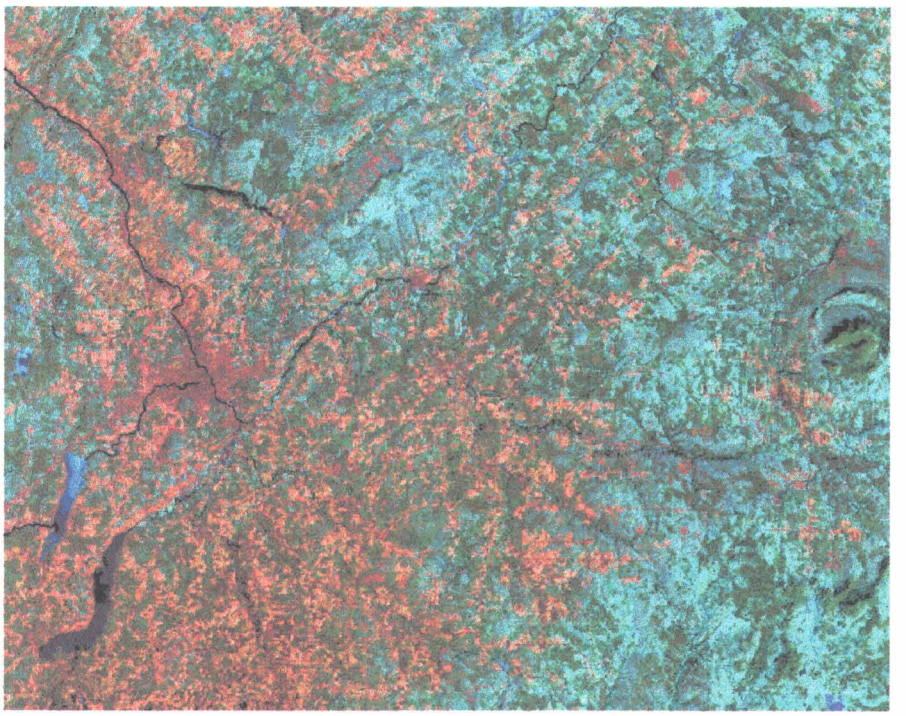

a) HRVIR bands (HRVIR4, HRVIR3, HRVIR2)

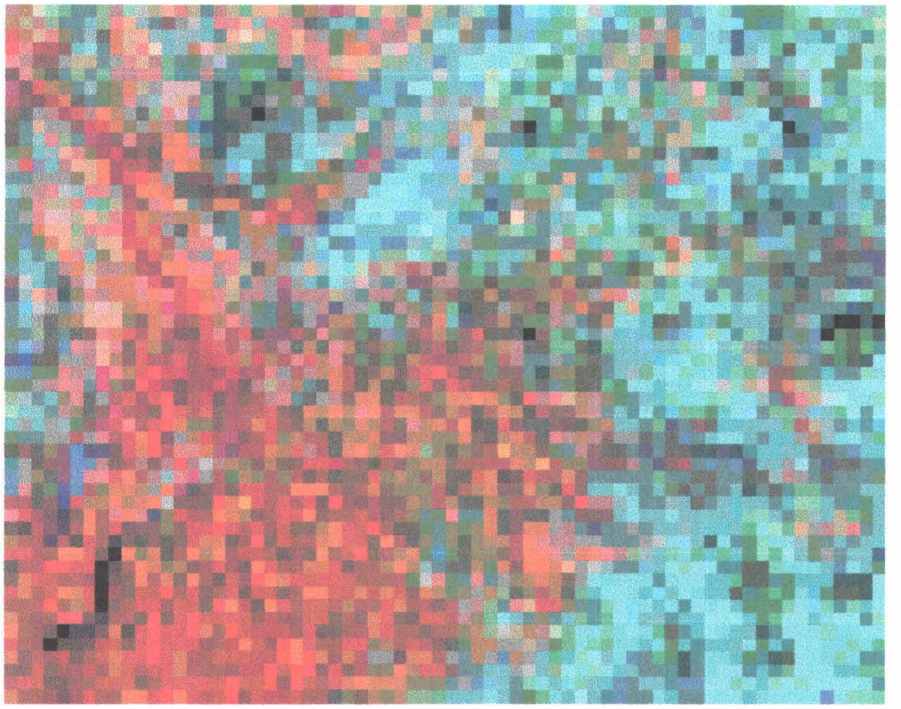

b) VGT bands (VGT4, VGT3, VGT2)

Figure 6.4: Simulated false color composites of HRVIR and VGT bands - April 2, 1988

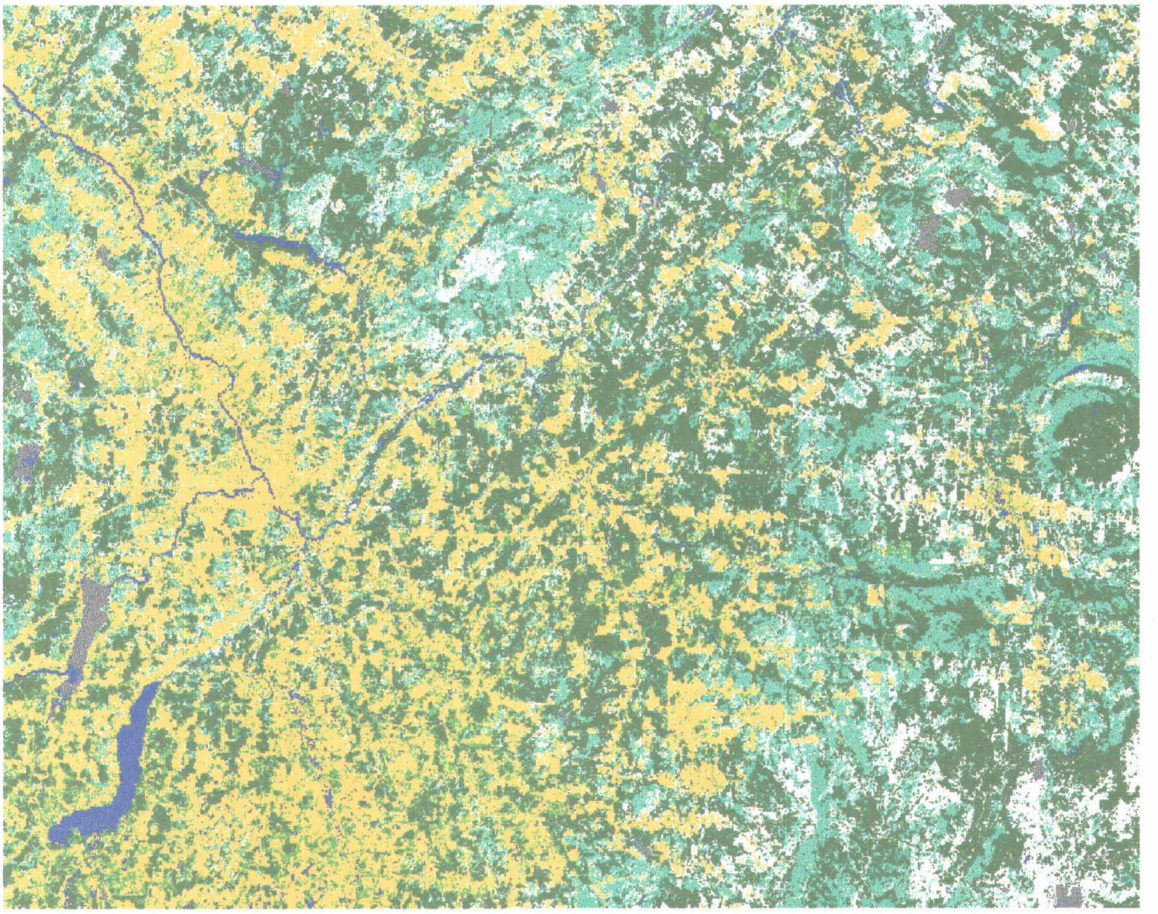

Figure 6.5: Classified HRVIR image - April 2, 1988

Table 6.1 Mean reflectances (standard deviation) and percentage of occupation of each identified land use classes on the spring image (April 2, 1988).

Land use classes	% of land use occupation	Reflectances (%)							
		HRVIR1		HRVIR2		HRVIR3		HRVIR4	
		Mean (%)	SD (%)	Mean (%)	SD (%)	Mean (%)	SD (%)	Mean (%)	SD (%)
Coniferous forest (with snow)	27.1	10.8	5.3	10.5	4.9	26.5	4.6	8.8	1.5
Coniferous forest (without snow)	0.0								
Deciduous forest (with snow)	21.1	26.1	7.2	28.0	7.1	35.7	5.6	9.7	1.6
Deciduous forest (without snow)	5.7	9.4	3.0	10.6	2.9	26.9	3.7	19.1	5.0
Open areas (with snow)	19.1	32.5	13.2	34.6	13.1	44.4	10.2	11.3	5.1
Open areas (without snow)	24.4	13.8	4.4	17.0	4.6	29.7	7.4	28.9	9.0
Lakes and rivers (frozen)	0.7	50.4	11.5	47.8	11.0	33.2	10.0	1.9	0.8
Lakes and rivers (unfrozen)	1.9	12.7	8.3	12.7	7.8	12.9	6.8	5.5	3.8

6.3 Sub-pixel estimation of snow cover

The difficulties that would likely be encountered for the estimation of snow cover on each individual land use class present on a single VGT pixel have been discussed in section 2.4.1. In particular, it was mentioned that the estimation of those percentages would be possible only if the reflectances were known and the number of endmembers, that is of land use classes, would be in agreement with the number of independent bands. In practice, those conditions were not satisfied with the image that we had and no worthwhile results could be obtained. There were more land use classes than bands. Also, open areas, which could be integrated into only one snow covered class, were sub-divided into more classes for snow free conditions. At the moment, no final conclusion can be reached concerning the possibility of estimating the percentages of snow cover on each land use class present in a specific pixel, using the mixing theory and only one VGT image. Areas with only one or two land use classes could possibly be considered. Also, there is the possibility of using more than one VGT image during a cold spell occuring in the melt period and keeping the percentages of snow covered and snow free areas constant for a few days.

There is however the possibility of finding the total percentage of snow cover on each pixel using either equation 2.11 or 2.12. Let us look mostly at the results from equation 2.11. Equation 2.11 is based on the assumption that the reflectance of a partially snow covered pixel will lie somewhere between that corresponding to snow free conditions and that corresponding to snow covered conditions. In normal operations, single VGT images or mosaics corresponding to those conditions would be available. In our case, no such images were of course available, so we have created them using the mean class reflectances of table 6.1 (figure 6.6) and the mixing theory. It should be clear that these images represent only an approximation of the images that should be used to apply equation 2.11 and that approximation should be felt on the results.

In figure 6.7a, the total percentage of snow cover on each pixel as obtained from equation 2.11, that is the value of F, is compared to the total percentage of snow cover on the same pixel as obtained from the HRVIR pixels corresponding to that VGT pixel. It can be seen that equation 2.11 underestimates the "true" percentage of snow cover on each pixel, but that a relation could be obtained with a coefficient of determination of 0.8377. Other relations could be obtained by not

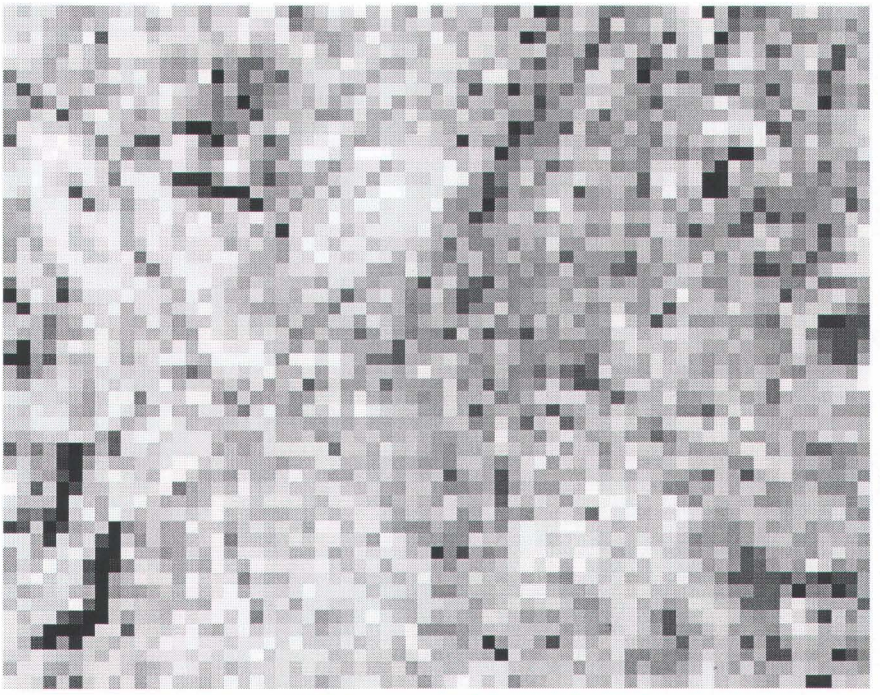

a) Simulated snow free VGT image (VGT4, VGT3, VGT2)

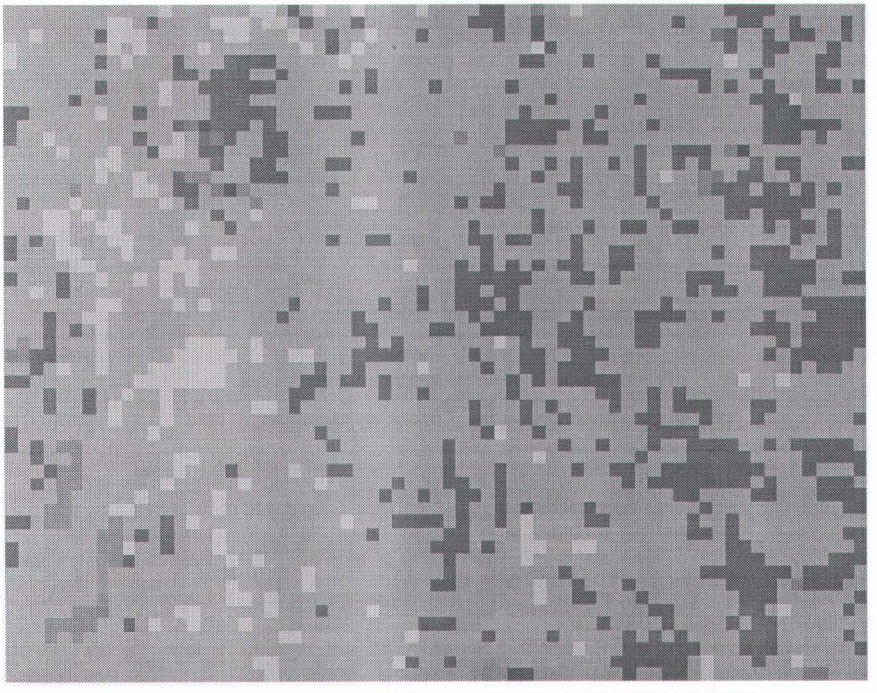

b) Simulated snow covered VGT image (VGT4, VGT3, VGT2)

Figure 6.6: Simulated false color composite images of the VGT bands.

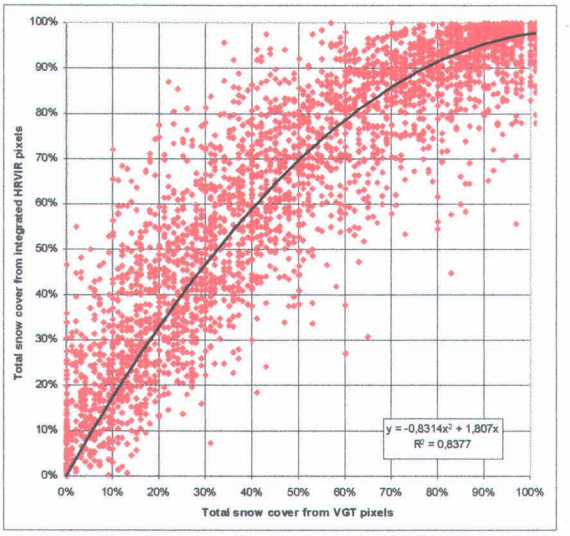

a) Total percentage of snow cover estimated from integrated HRVIR pixels as a function of the total snow cover estimated from VGT pixels (equation 2.11)

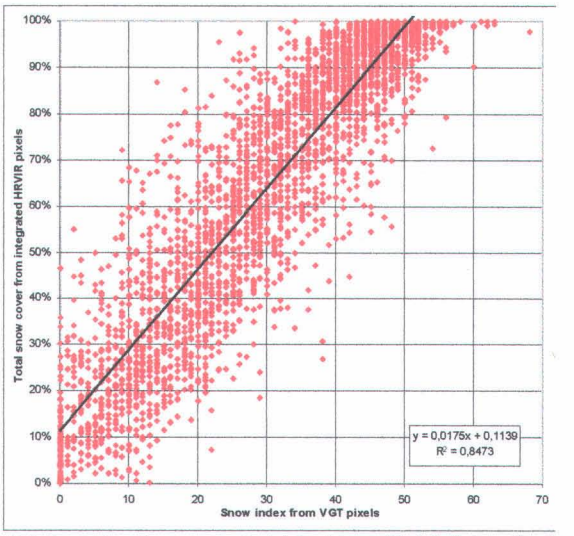

b) Total percentage of snow cover estimated from integrated HRVIR pixels as a function of the normalized difference snow index (NDSI) of equation 2.12.

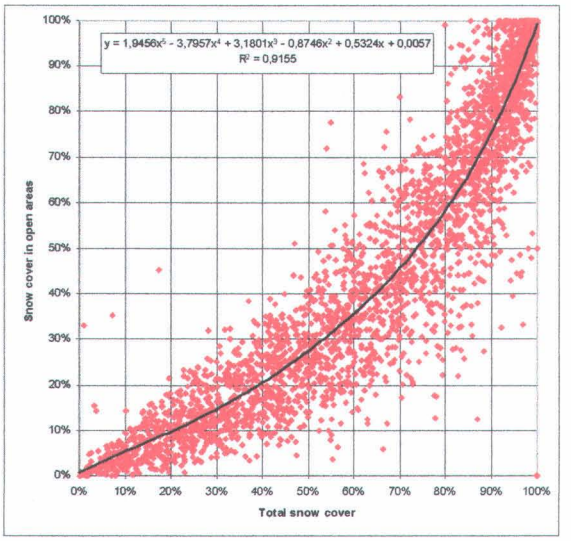

c) Percentage of open areas covered by snow on each VGT pixel as a function of the total area covered by snow on that pixel.

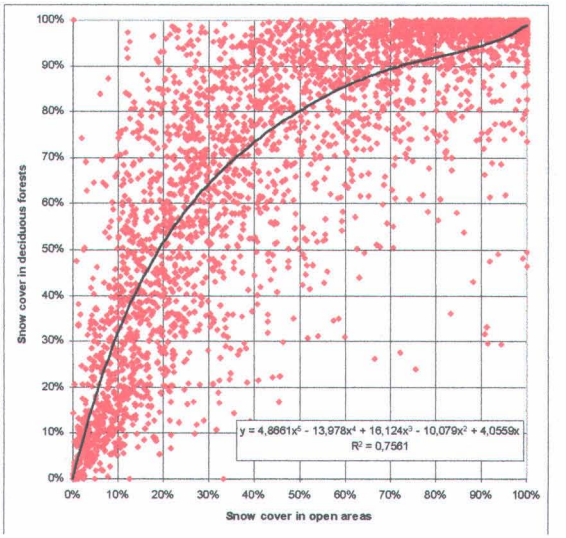

d) Percentage of deciduous forests covered by snow on each VGT pixel as a function Open areas covered by snow on that pixel.

Figure 6.7: Snow cover estimations on VGT pixels.

forcing the relation to go through (0,0) and/or using higher degree polynomials. It should be mentioned that 3672 points are on that figure and that the use of actual VGT images and not of images created from mean reflectances values, should normally lead to a smaller spread of the points on both sides of the relation.

The relation between the normalized difference snow index (NDSI) obtained from equation 2.12 and the total percentage of snow cover on the same pixel, as estimated from the HRVIR pixels corresponding to that VGT pixel, is presented in figure 6.7b. It can be seen that it is linear and has a coefficient of determination of 0.8473, which is very close to that of the previous relation. As a temporary conclusion, it can be said that both relations will likely furnish total snow cover on each pixel with approximately the same accuracy and that accuracy should be better with actuel VGT images.

It is however possible to try to distribute that total snow cover on each pixel among each of the mean land use classes, namely coniferous forests, deciduous forest and open areas. It is clear from observations and simulation of the melt process that snow disappears first in open areas, then in deciduous forests and finally in coniferous forests. It is thus likely that, for a given percentage of snow cover on a pixel, the remaining percentage of snow in forested areas will be greater than that in open areas. This is effectively shown in figures 6.7c and 6.7d.

In figure 6.7c, the percentage of snow cover in open areas on a specific VGT pixel is shown as a function of the total percentage of snow cover on that same pixel. If all VGT pixels would correspond to only one class, namely open areas more or less at the same elevation, then all points would lie on the $y = x$ curve. Since, in our case, a large number of VGT pixels are likely to include the three main land use classes, for each of these pixels, the percentage of snow covered HRVIR pixels corresponding to the open areas class will be lower than that corresponding to the total percentage of snow covered HRVIR pixels corresponding to a VGT pixel. This is what is shown in figure 6.7c. As an example, if the total snow cover on a pixel is 40%, than the snow cover in open area is down to 20%.

Let us look now at the relation between the snow cover in deciduous forests as compared to that in open areas, which is shown in figure 6.7d. It should be remembered here that it was impossible to find out snow free coniferous forests. One can notice readily that as the percentage of snow cover in open areas diminishes from 100% to, let us say, 50%, the percentage of snow cover in deciduous forested areas remains practically between 100% and 90% and, then, drops to zero as the percentage of snow cover continues to diminish in open areas. This behaviour confirms our assumptions. A fifth degree polynomial has been fit to the data as an example of a possible relation, but a number of other relations could be possible. For instance, we could have the percentage of snow cover in deciduous forested areas stay at 100% as long as the percentage of snow cover in open areas is greater than 50%, followed by a linear decrease to 0% from then on. It should be mentioned, finally , that a number of percentages of snow cover in deciduous forested areas are lower than the corresponding percentages in open areas. That should not be the case. The most probable reason for that is that pixels were improperly classified either in one class or the other. Fallow lands and bushes would probably be in that case.

It is finally interesting to present the information contained in figure 6.7a on a map rather than on a graph. Figure 6.8a represents the total percentage of snow cover on each VGT pixel, from 0 to 100%, as estimated from HRVIR pixels corresponding to each VGT pixel. It can be seen that complete snow cover correspond to the blue pixels in figure 6.4b, whereas the snow free areas are shown in reddish colors in that same figure. The total snow cover estimated by equation 2.11 is presented in figure 6.8b. It was mentioned previously that equation 2.11 was underestimating the percentage of snow cover on each VGT pixel and that is noticeable in figure 6.8b, as the grey shades are darker than in figure 6.8a. One can also mention that underestimation tends to occur mostly where the percentage of snow is relatively low. If the relation between total snow cover from equation 2.11 and total snow cover from HRVIR pixels, as determined in figure 6.7a, is applied, then the resulting map is shown in figure 6.8c. It can be seen that this latter map is much more similar to that of figure 6.8a. The absolute estimation error of the snow cover mapping in figure 6.8c in relation to the value of figure 6.8a is shown in figure 6.8d. It can seen that most of the snow cover estimations are within 10% of the HRVIR estimated values. More precisely, we have:

- Underestimation greater than 25% for 4.1% of the pixels;
- Underestimation between -25% and -10% for 10.3% of the pixels;
- Estimation within -10% and +10% for 70.1% of the pixels;

a) Estimated snow cover from HRVIR

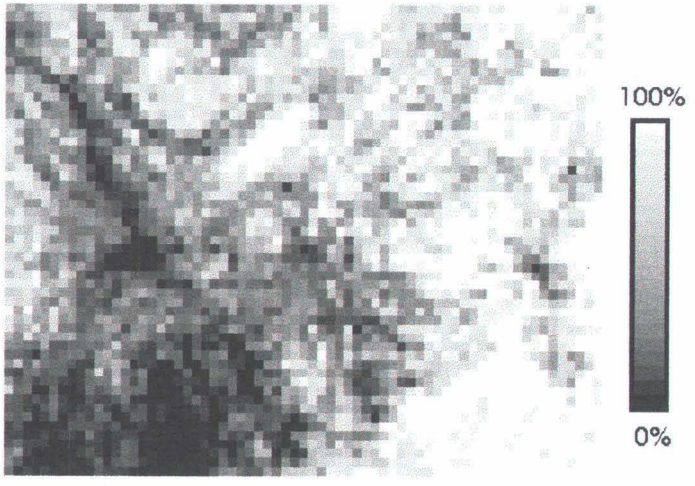

b) Estimated snow cover from VGT2 (equation 2.11)

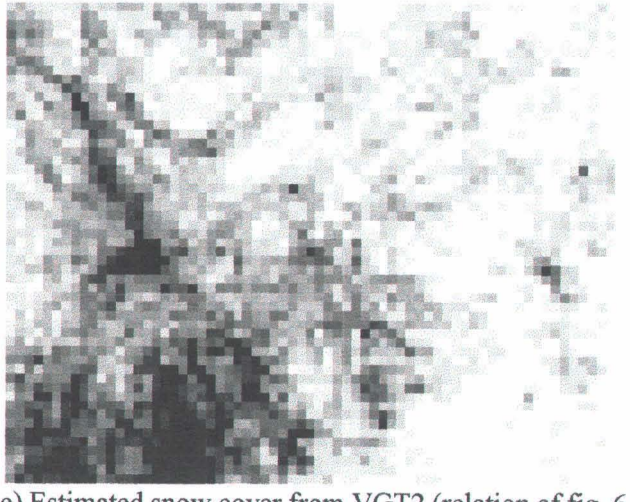

c) Estimated snow cover from VGT2 (relation of fig. 6.7a)

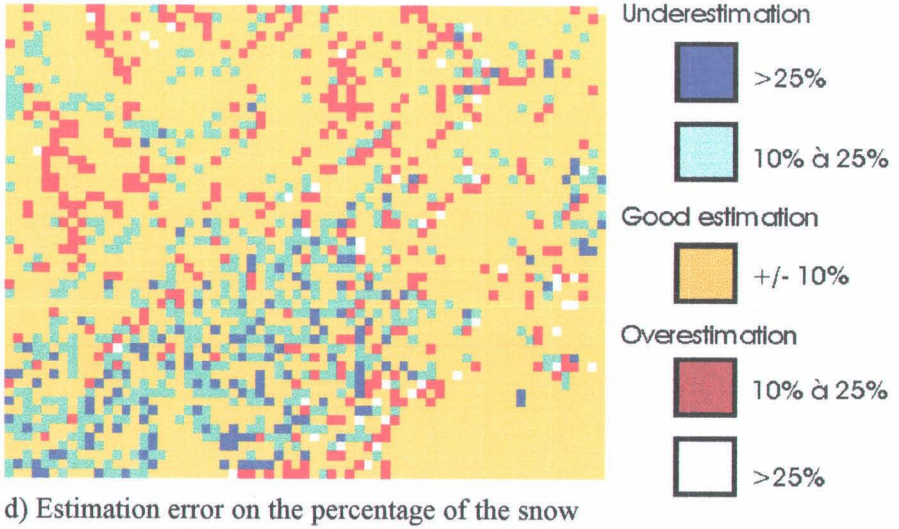

d) Estimation error on the percentage of the snow cover on each VGT pixel (fig. 6.8c - fig. 6.8a)

Figure 6.8: Snow cover estimation - April 2, 1988

- Overestimation between +10% and +25% for 10.3% of the pixels;
- Overestimation greater than 25% for 1.4% of the pixels.

The results obtained on snow cover estimation show that it is possible to estimate the total percentage of snow cover on each VGT pixel with a quite satisfactory accuracy, an accuracy than should be even better with actual data. It was also shown that it could be possible to go one step further in distributing that total snow cover among the main land use classes present on any VGT pixel. That possibility to estimate the spatial distribution of snow cover at the sub-pixel level will be very useful for hydrological simulations.

7 POST-LAUNCH ANALYSIS OF ACTUAL VGT AND HRVIR DATA

The pre-launch analysis of simulated VGT and HRVIR data has shown that it was possible to locate VGT images well within 100m, given a detailed land use map. It was further shown that estimating, thus monitoring, the mean reflectances of the land use classes present in a specific region from a VGT image was also possible, given a detailed land use map. Estimation of the total snow cover on each VGT pixel was also possible.

In the post-launch phase, we intend to test these findings with actual VGT and HRVIR data.

7.1 Monitoring of mean land use reflectances under snow free conditions

Monitoring of mean land use reflectances under snow free conditions needs the application of the procedure explained in chapter 2 and applied in chapter 5, on the area common to a VGT and a HRVIR image. Simultaneous acquisition of both VGT and HRVIR images is assumed at least once.

Given simultaneously obtained VGT and HRVIR images, we will first proceed to the classification of the HRVIR image in order to get the reference land use map necessary for the remaining procedures that will be applied to the common area. Next, we will test if the optimal number of groups of pixel found in the pre-launch phase does change or not. We will then be in a position to determine the location of the VGT image relative to the HRVIR image with an accuracy that we hope as good as in the pre-launch phase. Once this will be done, it will remain to estimate the mean reflectances of each of the selected land use classes and compare them to the mean reflectances estimated from the HRVIR image, with the objective that the VGT estimated reflectances will be within the standard deviations characterizing the mean reflectances values.

That procedure will be repeated for each of the VGT images that will be obtained to describe the variation of the reflectances with time as well as to prepare a data base of reflectances that will be

used in the next step. Spectrally integrated reflectances will subsequently be used as time varying albedo values of land use classes for our hydrological model HYDROTEL.

That next step will consist in reversing the spectral mixing relation in order to find out the percentages of land use classes on each of the VGT pixels in a region larger than the HRVIR image and including it, whereas still being relatively homogeeous as far as land class reflectances are concerned. This will need data from enough VGT images to be able to obtain as many equations as there are land use classes as explained in chapter 2. The result of this procedure will be an estimation of the percentages of each of the land use classes present in that larger region for each of the VGT pixels, but without knowledge of the position of these classes within the VGT pixels.

In short, we will test the developed procedure on actual VGT and HRVIR data as far as the accuracy of location and reflectance estimations are concerned and, finally, we will determine the percentages of land use classes for a region larger than the HRVIR image.

7.2 Monitoring of snow cover

Simulating the variation of snow cover both in time and space with an hydrological model, in order to be able to forecast snowmelt as accurately as possible, requires input data such as albedo. It should be remembered that albedo controls, at least partly, the flow of solar radiation into the snow cover. Also, albedo varies with time, old snow having a lower albedo than fresh snow. A ripe snow cover has a relatively low albedo.

We want, first, to monitor reflectances of land use cover over complete snow covers until the beginning of melt in spring. In particular, we want to verify to what extent it is possible to distinguish between an old and cold snow cover and a ripe snow cover. For that purpose, we will use informations coming both from the VGT image and from our distributed hydrological model HYDROTEL (Fortin *et al.*, 1995).

Once the melting process is in progress, the snow cover will disappear following a pattern related to geographical location, altitude and land use. A distributed hydrological model like our can simulate this process from the available input variables. As these variables are not necessarily

perfectly representative of the conditions throughout a watershed and no hydrological model is perfect, it is likely that the simulation of the snow cover will benefit from an update of the state variable of the model. Then, it becomes important to be able to monitor partial snow cover on a watershed during the melt period.

We intend to monitor total snow cover on each VGT pixel according to the procedure outline in chapter 2 and applied in chapter 6. We will also try to distribute the total snow cover on each VGT pixel among the land use classes present on that pixel also following the same procedure. This redistribution will need the acquisition of a HRVIR image to verify the resulting distribution.

At the moment, we believe that it will be difficult to apply the spectral mixture theory to obtain directly the percentage of snow cover on each of the land use classes present on a watershed as this will be a function of both the actual melting conditions and of cloud cover. If the right conditions are obtained, we will test that theory.

7.3 Data acquisition plan

7.3.1 General informations for actual SPOT-4 data

- Type of product: VGT-P and HRVIR multispectral
- Format: Standard SPOT format
- Support: CD-ROM or exabyte
- Maximum cloud cover: 20% (see below for details)
- Viewing angle for HRVIR: normally quasi-vertical.

7.3.2 Chosen site and region

The chosen center of the HRVIR images is located in the region previously analysed in the pre-launch phase (long. 71°46' W; lat. 45°38 N), that is the region of the St.François watersheds. As mentioned before, that region is representative of the types of land uses that can be encountered in southern Québec. We can count on a good meteorological network and the HYDROTEL model is already applied on the Chaudière and the Eaton watersheds.

The VGT images should have the same center as the HRVIR images (long. 71°46' W) in the E-W direction in order to have a similar quasi-vertical view of the area. In the N-S direction, the southern limit should at least be 43° N, which is two degrees south of the US-Canada border in that region. For the northern limit of the VGT images, it would be pertinent if it can go as far north as 56° N. That northern limit will allow coverage the James Bay watersheds in which we are developing a methodology for the estimation of the water equivalent and the extension of the snow cover using RADARSAT images. We already have a large coverage of high resolution land use classes in that second region so that it would not be necessary to procced to the acquisition of HRVIR data. If possible, actual HRVIR data would, of course, be very much appreciated to control our results but will not be asked within this project. We believe that the acquisition of VGT images will complement the informations coming from RADARSAT data, so that both types of data will likely be used for operational purposes. This RADARSAT project is supported by the ADRO program (Canadian Space Agency) and Hydro-Québec.

7.3.3 Number of images and temporal distribution

From the informations that we have on the types of products that will be available and the procedures that we have developed in the pre-launch phase, we have considered that VGT-P products would satisfy our needs. This being said, **we want to wait until the VGT-P products are in their final status as far as both radiometry and geometry are concerned, since we need those to be as good as possible on the original images.** The acquisition of the first VGT and HRVIR images will be conditionned by these needs. This is the reason why, in table 7.1, data acquisition starts in September 1998.

Table 7.1 Data acquisition

Month	Application	HRVIR		
		number	Center	VGT number
●Early September 98 or August 99	●Reflectances over full summer vegetation	1	71°46'W; 45°38'N	1*
●Late September 98 or 99	●Reflectances over colorfull fall vegetation			1*
●Late October 98 or 99	●Reflectances over late fall vegetation prior to the first snowfall, with leaves fallen in deciduous forested areas. Reference fall image for partial snow cover relation.			1*
●January to March 99	●Reflectance of snow cover (fresh and cold snow conditions)			1*
●January to March 99	●Reflectances of snow cover (cold snow at least a week old)			1*
●Late March-Early April 99	●Reflectances of complete snow cover at the very beginning of snowmelt			1*
●April 99	●Total percentage of snow cover on each VGTpixel, with partial snow cover in the region. Reflectances of snow cover (melting or cold) and of snow free areas.	1	Either of the other two locations	1*
●Late April-Early May 99	●Reflectances over snow free early spring vegetation. Reference spring image for partial snow cover relation.			1*
●Mid June 99	●Reflectances over summer vegetation. Test for estimation of percentages of land use classes outside the first HRVIR image	1	71°29'W; 46°26'N	1*
Total number of images		3		9

Note: The "*" has two significations. First, in the E-W direction, the center should be 71°46' W. In the N-S direction, it should go from from 43°N to 56°N. More details on the number of VGT images are given in section 7.3.3.

Normally, one VGT image will be sufficient for each indicated period. However, because of cloud cover, it may be necessary to rely on more than one image to cover the region of interest and prepare a mosaic of more than one image. Also, although only one VGT image is asked over partial snow cover, it would be interesting to have more, if possible, for a better test of snow cover monitoring in that crucial period. For snow free conditions, four or five VGT images would be a minimum, allowing to test the possibility to monitor reflectance variation over various land use classes, whereas, at the same time, providing the necessary data for the estimation of the percentages of land use classes outside of the areas covered by the first HRVIR image. The second HRVIR image (whose acquisition is planned for June 1999) would permit to check the accuracy of the percentages estimated from VGT images outside the first HRVIR image. Both that second image and the first one are located within the region covered by the TM image of 28th of August 1995 (Fig. 5.1).

Finally, a HRVIR image taken simultaneouly to a VGT image over partial snow cover would allow to verify the accuracy of the developed procedure with actual data. We can just hope that such conditions will be possible, given the revisit frequency of SPOT-4 and cloud cover. In order to make the realization of these conditions easier, the location of that HRVIR image could correspond to either of the two previous images.

We will of course need to know in advance the exact dates of data acquisition of all images, in order to obtain the required field information. We assume that this subject will be discussed later on.

8 CONCLUSION

The specific objectives of our investigation were (a) the estimation of physical variables of the surface, corresponding to each land cover within the pixel, the albedo for example, (b) the estimation at the sub-pixel level of the spatial distribution of snow cover on the ground and (c) a positionning of the images as accurate as possible for multitemporal input into a spatially distributed hydrological model using geocoded data.

These three specific objectives have been reached for the analysis of simulated VGT and HRVIR data in the pre-launch phase of the project. As shown in the procceding chapters, it has been possible to locate the position of simulated VGT images well within 100m. Within that distance from the "true" position, the estimations of the mean reflectances of the land use classes are not significantly affected, so that it is quite acceptable to be able to get such a geometric accuracy. Also, it has been possible to estimate the total percentage of snow cover within each simulated VGT pixel, so that it was possible to map the spatial distribution of snow cover at the sub-pixel level.

As the actual VGT images should have better radiometric characteristics than those of the simulated images and we were obliged to create synthetic images for the snow cover procedure, we consider that we should be able to reach as good, if not better, results with the actual VGT and HRVIR images. For that purpose, the procedure that we intend to follow, together with the data acquisition plan that we suggest, have also been explained in the preceeding chapter.

The various results that will come from the analysis of the VGT and HRVIR data in southern Québec will be used as input to our distributed hydrological model HYDROTEL. The northern part of the VGT images will be used in the project that we have in northern Québec and may lead to operational use of VGT images, together with RADARSAT and SSM/I images over the James Bay watersheds, for snow cover monitoring and input to HYDROTEL.

9 BIBLIOGRAPHY

Aman, A, Randriamanantena, H.P., Podaire, A. and R. Frouin (1992). Upscale Integration of Normalized Difference Vegetation Index: The Problem of Spatial Heterogeneity, IEEE Trans. on Geoscience and Remote Sensing, 30(2): 326-338.

Cherchali, S. (1995). Contribution à la résolution du problème du pixel mixte en vue de l'amélioration de l'estimation de la productivité primaire nette en zone sahélienne (couplage haute et basse résolution spatiale). Thèse de doctorat, Université Paul-Sabatier, 232p.

Fortin, J.P., Moussa, R., Bocquillon, C. et J.P. Villeneuve (1995). Hydrotel, un modèle hydrologique distribué pouvant bénéficier des données fournies par la télédétection et les systèmes d'information géographique. Revue des Sciences de l'Eau, 8: 97-124.

Guyot, G. and Xing-Fa Gu (1994). Effect of Radiometric Corrections on NDVI-Determined frim SPOT-HRV and Landsat-TM Data. Remote Sens. Environ. 49:169-180.

Justice, C.O., Markham, B.L., Townshend, J.R.G. and R.L. Kennard (1989.) Spatial Degradation of Satellite Data, Int.J. Remote Sensing, 10(9): 1539-1561.

Kerdiles, H. and M.O. Grondona (1995). NOAA-AVHRR NDVI decomposition and subpixel classification using linear mixing in the Argentinean Pampa. Int. J. Remote Sensing, 16(7): 1303-1325.

Kneizys, F.X., Chetwynd, J.H., Clough, S.A., Shettle, E.P., Abreu, L.W., Frenn, R.W., Gallery, W.O and J.E.A. Selby (1983). Atmospheric Transmittance/Radiance computer code LOWTRAN 6. Optical Physics Division, Air-Force Geophysics Laboratory, Bedford, Massachuesetts, U.S.A. 200 p.

Kneizys, F.X., Shettle, E.P., Abreu, L.W., Chetwynd, J.H ., Anderson, G.P., Gallery, W.O., Selby, J.E.A and S.A. Glough (1988). Guide to LOWTRAN-7. AFGL-TR-88-0177, Air-Force Geophysics Laboratory, Bedford, Massachuesetts, U.S.A.

Novo, E.M. and Y.E. Shimabukuro (1997). Identification and mapping of the Amazon habitats using a mixing model. Int. J. Remote Sensing, 18(3): 663-670.

Rahman, H. and G. Dedieu (1994). SMAC: a simplified method for the atmospheric correction of satellite measurements in solar spectrum, Int. J. Remote Sensing, 15(1): 123-143.

Richter, R. (1989). Model SENSAT-3, DLR-IB 552/06 89, German Aerospace Research Establishment, Wessling, F.R. Germany.

Shimabukuro, Y.E., Carvalho, V.C. and B.F.T. Rudoff (1997). NOAA-AVHRR data processing for the mapping of vegetation cover. Int. J. Remote Sensing, 18(3): 671-677.

Simpson, J.J., Stitt, J.R. et M. Sienko (1998). Improved estimates of the areal extent of snow cover from AVHRR data. Journal of Hydrology, 204: 1-23.

Tanré, D., Deroo, C., Duhaut, P., Herman , M., Morcrette, J.J. Perbos, J. and P.Y. Deschamps (1990). Description of a computer code to simulate the satellite signal in solar spectrum: The 5S code. Int. J. Remote Sensing, 11: 659-668.